# Neutrophils homing into the retina trigger pathology in early age-related macular degeneration

Sayan Ghosh[1], Archana Padmanabhan[2], Tanuja Vaidya[2], Alan M. Watson[3], Imran A. Bhutto[1],

Stacey Hose[1], Peng Shang[1], Nadezda Stepicheva[1], Meysam Yazdankhah[1], Joseph Weiss[1],

Manjula Das[4], Santosh Gopikrishna[2], Aishwarya[2], Naresh Yadav[2], Thorsten Berger[5],

Tak W. Mak[5], Shuli Xia[6], Jiang Qian[7], Gerard A. Lutty[7], Ashwath Jayagopal[8],

J. Samuel Zigler, Jr.[7], Swaminathan Sethu[2], James T. Handa[7], Simon C. Watkins[3],

Arkasubhra Ghosh[2] and Debasish Sinha[1, 3, 7*]

[1]Department of Ophthalmology, University of Pittsburgh School of Medicine, Pittsburgh, PA. ,

[2]Narayana Nethralaya Foundation, Bengaluru, India, [3]Center for Biologic Imaging and

[3]Department of Cellular Biology, University of Pittsburgh School of Medicine, Pittsburgh, PA.,

[4]Beyond Antibody, Bengaluru, India, [5]The Campbell Family Institute for Breast Cancer

Research and Ontario Cancer Institute, University Health Network, Toronto, ON, Canada, [6]Hugo

W. Moser Research Institute at Kennedy Krieger, Department of Neurology and [7]The Wilmer

Eye Institute, The Johns Hopkins University School of Medicine, Baltimore, MD., [8]Pharma

Research and Early Development, Roche Innovation Center, F. Hoffmann-La Roche, Ltd., Basel,

Switzerland.

**Corresponding author:** Debasish Sinha, Departments of Ophthalmology, Cell Biology and

Developmental Biology, Children's Hospital of University of Pittsburgh School of Medicine,

One Children's Hospital Drive, 4401 Penn Avenue, Pittsburgh, PA 15224.

Email: Debasish@pitt.edu

**Abstract**

Age-related macular degeneration (AMD) is an expanding problem as longevity increases worldwide.  Inflammation contributes to vision loss in AMD, but the mechanism remains controversial.  We show neutrophil infiltration into retinas of early AMD patients and a mouse model with an early AMD-like phenotype.  Specifically, we observed increased levels of IFNλ in early AMD triggering neutrophil activation and lipocalin-2 (LCN-2) upregulation.  NOD-SCID immune-deficient mice were injected intravenously with IFNλ− activated dye labeled normal neutrophils and ribbon-scanning confocal microscopy (RSCM), showed the neutrophils infiltrating the eye.  Infiltration was greatly reduced when LCN-2$^{-/-}$ neutrophils were used. LCN-2 promotes inflammation and AMD-like pathology by interacting with Disabled homolog2 (Dab2) and modulating integrin β1 levels to stimulate adhesion and transmigration of activated neutrophils into the retina.  Inhibiting AKT2 in the mouse model neutralizes IFNλ inflammatory signals, reduces LCN-2-mediated neutrophil infiltration and reverses early AMD-like phenotype changes, thereby providing a potential therapeutic target for early, dry AMD.

**Introduction**

AMD is a complex and progressive degenerative eye disease involving multiple genetic and environmental factors leading to severe loss of central vision[1]. The vast majority of patients suffer from early, dry AMD, and, about half of these patients will develop advanced disease within ten years. Despite the growing need, no definitive treatment or prevention for early, dry AMD is available. Inflammation plays a key role in the pathogenesis of various age-related diseases, including AMD[2-4]. Dysregulation of the innate immune system is critical for the onset of AMD; complement has been implicated, activation of various cytokines/chemokines, and the NLRP3 inflammasome have been invoked as central to AMD pathogenesis[5,6]. The inflammatory cells like microglia, monocytes/macrophages, and tissue-resident T cells, also appear to contribute to AMD pathobiology[7]. However, a role for neutrophils in AMD remains largely unexplored. In addition, the molecular mechanisms involved in immune system activation and regulation in AMD, and in the assembly of the inflammation-signaling platform, remain unknown.

Neutrophils play a central role in the innate immune response[8,9]. Our recent study revealed increased infiltration of LCN-2 positive neutrophils into the choroid and retina of early, dry AMD patients as compared to age-matched controls[10]. It is now accepted that neutrophil subtypes that migrate to affected sites play a significant role in disease pathogenesis[11]. LCN-2, a protein involved in innate immunity, has been shown to be markedly elevated in serum and tissues during inflammation[12]. We have previously shown that LCN-2 is significantly higher in RPE cells of the aging *Cryba1* (gene encoding βA3/A1-crystallin) cKO (conditional knockout)

66     mouse, although we found no difference in younger mice[13].

67

68          While the lack of a comprehensive animal model of AMD limits our understanding of

69     cellular mechanisms in the critical early disease stages, the mouse has been the model organism

70     most used to study AMD[14,15]. We recently developed a genetically engineered mouse model that

71     exhibits a slow progressive early, dry AMD-like pathology associated with inefficient lysosomal

72     clearance decreasing both autophagy and phagocytosis in the RPE[16,17]. In the *Cryba1* cKO

73     mouse, these impairments lead to RPE cell degeneration including loss of basal infoldings,

74     prominent intracellular vacuoles, and undigested melanosomes, as well as sub-retinal lesions at

75     the posterior pole, deposits between the RPE and Bruch's membrane, decreased

76     electroretinogram (ERG) signals, and photoreceptor degeneration as the disease progresses[13,16].

77     Our mouse model exhibits a slowly progressive form of AMD-like pathology associated with a

78     chronic inflammatory immune response as the mice age, allowing us to test our hypothesis that

79     infiltrating neutrophils homing to the retina during disease progression contribute to

80     pathogenesis in early, dry AMD.

81

82          We demonstrate elevated interferon−lambda (IFNλ) in the retinae of human AMD

83     subjects and in the *Cryba1* cKO mouse model. This high expression of IFNλ in AMD retina

84     signals the transmigration of neutrophils from the circulation into the retina during early AMD,

85     eventually leading to major pathological sequelae. Here, we present the first study on

86     mechanisms whereby neutrophils may be activated in early AMD by signaling through the

87     IFNλ/LCN-2/Dab2/integrin β1 axis. In the mouse model, inhibition of AKT2 reduced homing

88     of neutrophils to the retina, decreased IFNλ expression, and alleviated early RPE changes.

**Results**

91    *Infiltration of neutrophils in AMD and in a mouse model*

92

93          As in human AMD[10], *Cryba1* cKO mice present with immune cell infiltration into the

94    retina with aging (Fig. 1a).  Flow cytometry analysis for the entire retinal cell population from

95    posterior eyecups was performed by gating for $CD45^{high}CD11b^{+}$ cells (monocytes, macrophages,

96    and neutrophils).  The relative number of neutrophils (cells positive for $Ly6C^{high}Ly6G^{+}$) among

97    $CD45^{high}CD11b^{+}$ cells in the tissue was determined, by simultaneously labelling cells with

98    appropriate antibodies (Fig. 1a), as previously described[18].  While not increased in 2 month old

99    *Cryba1* cKO retina, by 4 months, when an AMD-like phenotype is apparent in this mouse model,

100    $CD45^{high}CD11b^{+}Ly6C^{high}Ly6G^{+}$ neutrophils were increased nearly 3-fold relative to *Cryba1*^{fl/fl}

101    control retinas, and continued to increase with age, as seen in the 13 month old *Cryba1* cKO

102    retina with respect to aged control mice (Fig. 1a).  Furthermore, immunofluorescent analysis of

103    retinal flatmounts from *Cryba1* cKO mice confirmed an elevated number of $Ly6G^{+}$ cells in the

104    retina relative to age-matched controls (Fig. 1b).  A significant increase in sub-retinal

105    neutrophils, as determined by $Ly6G^{+}$ staining of RPE flatmounts, was also observed in *Cryba1*

106    cKO mice relative to age-matched controls (Supplementary Fig. 1).

107

108          The percentage of neutrophils and their activation status in human early, dry AMD was

109    studied by phenotyping the cells in peripheral blood (Supplementary Table 1) by flow cytometry

110    using appropriate gating strategies (Supplementary Fig. 2).  An increase in the proportion of

111    $CD66b^{+}$ neutrophils within the total $CD45^{+}$ (leukocyte) population was observed in peripheral

112    blood (Supplementary Fig. 3a) of AMD patients compared to control subjects.  Further, an

113    increased number of activated neutrophils (CD45$^+$CD66b$^{high}$) was observed in peripheral blood

114    (Fig. 1c) with no change in the number of inactive neutrophils (CD45$^+$ CD66b$^{low}$)

115    (Supplementary Fig. 3b).  We also observed a significant increase in the total number of IFNλ

116    receptor (IL-28R1)-positive leukocytes (CD45$^+$IL-28R1$^+$) in the peripheral blood of AMD

117    patients (Fig. 1d).  Moreover, IL-28R1$^+$ activated neutrophils (CD66b$^{high}$) were a significantly

118    higher proportion of total neutrophils (CD66b$^+$ cells) in peripheral blood (Fig. 1e) from AMD

119    subjects compared to age-matched controls. Immunolocalization studies show presence of

120    CD66b$^+$ neutrophils in human tissue sections from normal and AMD samples (Supplementary

121    Figure 3ci-iv).  We have previously shown that an increased number of neutrophils are present in

122    the retina of human AMD patients compared to aged-matched control subjects[10].  However,

123    IL28R1$^+$ expression is evident on CD66b$^+$ neutrophils only in retinal sections of AMD patients,

124    but not in controls (Supplementary Figure 3ci-v), indicating that activated neutrophils home into

125    the retina of only early AMD patients.  These results indicate a greater propensity for IL-

126    28R1$^+$ activated neutrophils to home into the eye, giving a probable scenario for the role of

127    IFNλ-mediated signaling in these infiltrating neutrophils.  It is known that once in the area of

128    inflammation, neutrophils release Neutrophil Extracellular Traps (NETs), which can damage

129    host tissue in immune-mediated diseases[19-22].  Indeed, early, dry AMD eyes showed increased

130    staining for the NET markers, myeloperoxidase (MPO), neutrophil elastase and citrullinated

131    histone H3 as compared to age-matched control eyes (Supplementary Fig. 4ai-iii & bi-iii).

132    Taken together, our results support the idea that there is increased neutrophil infiltration into the

133    retina during early, dry AMD.

134

*Factors promoting neutrophil infiltration into the retina*

RNAseq analysis was performed on retinal tissue obtained from 5 and 10 month old *Cryba1* cKO and floxed control mice in order to identify soluble factors, including cytokines and chemokines released from the retina, that may promote neutrophil infiltration. We found a significant increase in the levels of IFNs, including IFNα, IFNγ and IFNλ, as well as CXCL1 and CXCL9, in the aged *Cryba1* cKO retinas compared to control (Supplementary Fig. 5). ELISA was performed to further confirm these results (Fig. 2ai-iii). Furthermore, to identify which cell types express IFNλ in the retina, immunofluorescence studies were conducted and showed significantly increased staining for IFNλ specifically in the RPE of AMD eye sections relative to age-matched controls (Supplementary Fig. 6). Moreover, western analysis confirmed increased IFNλ and CXCL1 protein in human AMD RPE/choroid lysates, compared to control (Fig. 2b). In addition, we observed an increase in the levels of IFNα and IFNλ1 in the plasma and AH of early AMD patients compared to controls (Fig. 2c-f), but levels of IFNλ2/3 were not different in AMD patients compared to controls (Fig. 2g-h). The plasma levels of IFNγ showed significant increase in AMD patients compared to control (Supplementary Fig. 7a), but no such change was found in the AH (Supplementary Fig. 7b). IFNβ and VEGF levels in the plasma and AH of AMD patients did not show any significant change relative to control (Supplementary Fig. 7c-f). Thus, our results suggest a pro-inflammatory milieu in the eye, with a probable involvement of IFNλ, which is secreted from the diseased RPE thereby eliciting an inflammatory response. It is plausible that the increased levels of IFNλ might be the key factor that promotes the neutrophil activation and infiltration into the retina, since IFNλ receptor (IL28R1) is expressed on circulating neutrophils.

158

159     In addition to soluble factors, neutrophils also require adhesion molecules for their

160     transmigration into the site of injury.  Neutrophils adhere to endothelial cells when their integrins

161     interact with endothelial cell immunoglobulin superfamily members[23], such as ICAM-1 and

162     VCAM-1 (two important adhesion molecules on endothelial cells)[24,25], which enables them to

163     transmigrate into diseased or injured tissue.  We observed elevated levels of ICAM-1 (Fig. 2i) as

164     well as VCAM-1 (Fig. 2j) in the retina of aged *Cryba1* cKO mice and human early, dry AMD

165     patients respectively, relative to age-matched controls.

166

167     *IFNλ triggers LCN-2 expression and neutrophil activation*

168

169     It has been previously reported that IFNλ triggers phosphorylation and nuclear

170     translocation (activation) of STAT1[26].  We have shown that during early AMD, STAT1

171     activation is critical for LCN-2 gene expression[10].  LCN-2 is an adipokine, known to be

172     important for neutrophil activation and innate immune function[27].  In fact, we and others have

173     shown that binding of NFκB and STAT1 to the promoter of LCN-2 causes pathogenicity[10,28].

174     Here, we show that mouse bone marrow-derived neutrophils cultured with either recombinant

175     IFNλ or with conditioned medium from primary cultured RPE cells overexpressing IFNλ to

176     simulate the increased IFNλ levels that we observe in the RPE of human AMD patients

177     (Supplementary Fig. 6), exhibit increased levels of LCN-2 and phosphorylated STAT1 (Fig. 3a).

178     Moreover, we also observed that IFNλ-exposed neutrophils showed a significant increase in

179     reactive oxygen species (ROS) levels (Fig. 3b) and phagocytosis (Fig. 3c).  Increased formation

180     of NETs was evident because of the prevalence of extracellular nuclear material (stained with

181 DAPI), which showed increased staining for myeloperoxidase (MPO) and citrullinated Histone

182 H3 (Fig. 3d), known markers of NETs[29]. Thus, the data suggests that IFNλ not only induces

183 STAT1-mediated LCN-2 expression, but also potentiates neutrophil activation.

184

185 *LCN-2 activated neutrophils cause outer retinal degeneration*

186 We applied ribbon-scanning confocal microscopy (RSCM)[30] as a means to rapidly image

187 red CMTPX-tagged neutrophils within an entire NOD-SCID immune-deficient mouse eye to

188 validate transmigration of activated neutrophils. The mice were intravenously injected with bone

189 marrow-derived wild type (WT) neutrophils, bone marrow-derived neutrophils from LCN-2$^{-/-}$

190 (knockout) mice, WT neutrophils treated with IFNλ, or IFNλ treated neutrophils from LCN-2$^{-/-}$

191 mice. To demonstrate homing of activated neutrophils to specific regions of the eye, we

192 performed RSCM paired with benzyl alcohol benzyl benzoate (BABB) clearing of NOD-SCID

193 mouse eyes. The clearing procedure makes the refractive index consistent throughout the eye,

194 thereby making the tissue transparent and allowing image acquisition throughout the depth of the

195 whole organ. As shown in Fig. 4, NOD-SCID mice administered with red CMTX-tagged WT

196 neutrophils showed little infiltration into the eye (Fig. 4ai-iv) and similarly, not many neutrophils

197 derived from LCN-2$^{-/-}$ mice infiltrated the eye (Fig. 4bi-iv). The data clearly suggest that

198 neutrophils home mostly into the choroid in both of these conditions, but due to the lack of

199 stimuli from IFNλ in WT neutrophils and probably due to the perturbed migratory signaling axis

200 in the LCN-2$^{-/-}$ mice, these cells fail to cross the intra-ocular compartments in considerable

201 numbers through the blood-retinal or blood-aqueous barrier. Interestingly, red CMTPX-tagged

202 neutrophils treated with IFNλ showed a noticeable number of neutrophils infiltrating the eye,

203 mostly into the retina (Fig. 4ci-iv & Fig. 5d) relative to control (Fig. 4ai-iv & Fig. 5d). A 3D

204  model shows the number and location of the infiltrating neutrophils in the eye (Fig. 5a-d &

205  Supplementary Movie 1).  We envisage that during early stages of AMD, neutrophils migrate

206  from the peripheral blood into the intra-ocular compartments in response to a chemotactic cue,

207  which we identified as IFNλ.  In addition, NOD-SCID mice injected with IFNλ–treated LCN-2$^{-/-}$

208  neutrophils showed very few infiltrating cells into the retina (Fig. 4di-iv) compared to mice

209  injected with untreated LCN-2$^{-/-}$ neutrophils (Fig. 4bi-iv), demonstrating that neutrophil

210  infiltration into the eye from the peripheral circulation is likely due to the IFNλ triggered LCN-2

211  activation.

212

213       To further validate our observations that increased LCN-2 levels induced by IFNλ in the

214  transmigrating neutrophils can potentiate outer retinal degeneration, we injected NOD-SCID

215  mice with bone marrow-derived WT neutrophils, bone marrow-derived neutrophils from

216  LCN-2$^{-/-}$ mice, WT neutrophils treated with IFNλ,  neutrophils treated with conditioned medium

217  from primary cultures of RPE cells overexpressing IFNλ, or with recombinant LCN-2.   After 7

218  days, Optical Coherence Tomography (OCT) analysis showed that mice injected with either

219  IFNλ-treated WT neutrophils or recombinant LCN-2 exhibited alterations in the RPE and

220  photoreceptor (inner and outer segments) layers (Fig. 6aiii-v). Quantitative analysis by spider

221  plot revealed decreased thickness of these layers in the experimental groups (Fig. 6aix and

222  Supplementary Fig. 8a). No significant changes were observed in mice treated with vehicle

223  and/or WT neutrophils (Fig. 6ai, ii and ix).  In addition, LCN-2$^{-/-}$ neutrophils, as well as LCN-2$^{-/-}$

224  neutrophils treated with IFNλ, showed no degenerative changes (Fig. 6avi-ix), suggesting a

225  pathogenic role of LCN-2 in retinal degeneration. Hematoxylin-eosin staining of retinal sections

226  from NOD-SCID mice, injected with either IFNλ-treated WT neutrophils or recombinant LCN-

227   2, showed degenerative changes in the outer nuclear layer (ONL) along with photoreceptor layer

228   (disruption of the inner and outer segments [IS/OS] junction) and RPE-Bruch's membrane-

229   choriocapillaris complex (Fig. 6biii-v), relative to vehicle control or WT neutrophil injected mice

230   (Fig. 6bi-ii).  Further, a thickness measurement of the retinal layers from these sections by spider

231   plot showed severe loss or thinning of IS/OS and RPE layers in mice injected with either IFNλ-

232   treated WT neutrophils or recombinant LCN-2, relative to vehicle or WT neutrophil-treated

233   groups (Fig. 6bix).  In addition, immunofluorescence studies confirm increased photoreceptor

234   and RPE cell loss in these mice, as evident from reduced staining for rhodopsin (labels rod

235   photoreceptors) and RPE 65 (retinal pigment epithelium-specific 65kDa protein) in the retina of

236   NOD-SCID mice, injected with either IFNλ-treated WT neutrophils or recombinant LCN-2

237   (Supplementary Fig. 8biii-v), with respect to controls (Supplementary Fig. 8bi-ii).

238    Therefore, our NOD-SCID mouse data provides novel evidence that IFNλ triggers LCN-2

239   activation in neutrophils, thereby inducing transmigration into the retina and potentiating retinal

240   degeneration.

241

242   *Association of LCN-2/Dab2 regulates neutrophil infiltration*

243

244          These observations prompted us to further investigate the possible molecular mechanisms

245   by which neutrophils infiltrate into the retina and thereby contribute to the pathogenesis of

246   AMD.  It has previously been shown that LCN-2 regulates neutrophil chemotaxis and cell

247   migration in cancer cells[27,31]. To ascertain if IFNλ-mediated LCN-2 activation in neutrophils

248   contributes to the increased adhesion and transmigration, we performed a human proteome high-

249   throughput array to identify LCN-2 binding partners that may play a specific role in cell

250    adhesion and migration.  We found that LCN-2 interacts with Dab2 (Supplementary Fig. 9).

251    This was confirmed by a pull-down assay, which showed an increased association between LCN-

252    2 and Dab2 in IFNλ-exposed neutrophils as compared to untreated or control conditioned media

253    treated neutrophils (Fig. 7a).   It has previously been reported that, Dab2 binds to integrin β1 and

254    regulates its internalization, thereby modulating cell migration[32].  It is also known that Dab2 is a

255    negative regulator of cell adhesion particularly during inflammation[33,34]. Moreover, extracellular

256    integrin β1 expression drives cell adhesion on the endothelial cell surface in various tissues

257    thereby facilitating transmigration into the tissue[35,36]. We hypothesized that this increased

258    association between LCN-2 and Dab2 may regulate extracellular integrin β1 level by modulating

259    the Dab2/integrin β1 axis, thereby promoting neutrophil adhesion and transmigration into the

260    retina.  To explore the novel role of LCN-2 we used bone marrow-derived neutrophils from WT

261    and LCN-2$^{-/-}$ mice that were cultured with either recombinant IFNλ or conditioned medium from

262    IFNλ overexpressing RPE cells.  Flow cytometry studies revealed an increase in extracellular

263    integrin β1 expression in IFNλ-exposed neutrophils from wild type mice (Fig. 7b & c)

264    concomitant with decreased of integrin β1 (Fig. 7d). In addition, our co-immunoprecipitation

265    data did not show any significant change in the binding between Dab2 and integrin β1 upon

266    IFNλ exposure (Supplementary Fig. 10).These results suggest towards an alteration in the Dab2-

267    mediated cellular internalization of integrin β1 in the IFNλ-exposed neutrophils, particularly due

268    to the increased association between LCN-2 and Dab2 in the IFNλ-exposed cells (Fig 7a).

269

270    Since we also observed neutrophils homing into the eye in NOD-SCID mice that were

271    injected with IFNλ-exposed LCN-2$^{-/-}$ neutrophils (Fig. 5a), it is likely that the expression of

272    adhesion-associated surface proteins is downregulated in the absence of LCN-2, as has been

273    shown previously[37].  Based on these observations, we postulate that LCN-2 regulates the

274    expression of extracellular adhesion molecules, which in turn modulates cell adhesion and

275    transmigration.  However, there could be involvement of putative redundant pathways in

276    regulating neutrophil infiltration upon exposure to IFNλ.  We observed intensified neutrophil

277    adhesion on fibrinogen-coated plates (Fig. 7e) and transmigration of IFNλ-treated normal

278    neutrophils across fibrinogen-coated transwell chambers (Fig. 7f).  In addition, we found that

279    there is an increase in the extracellular expression of integrin β1 on untreated neutrophils from

280    LCN-2$^{-/-}$ mice (Figure 7b and c). This data is in sharp contrast to our previous observation that

281    LCN-2$^{-/-}$ neutrophils treated with IFNλ has decreased surface expression of integrin β1 (Fig. 7b-

282    c). Previous studies have shown that integrin β1 surface expression in neutrophils can be

283    modulated by a number of independent signaling cascades during inflammation[38-41]. It is

284    therefore plausible that integrin β1 in untreated LCN-2$^{-/-}$ neutrophils is upregulated

285    independently of IFNλ/LCN-2/Dab2 pathway. But, the extracellular integrin β1 level and its

286    internalization were stabilized in these LCN-2$^{-/-}$ neutrophils, even after IFNλ treatment, relative

287    to IFNλ-exposed WT neutrophils (Fig. 7b-d).  However, the adhesion and transmigration

288    properties were significantly reduced in LCN-2$^{-/-}$ neutrophils exposed to IFNλ (Fig. 7e-f) and in

289    integrin β1 silenced normal neutrophils (Fig. 7e-f), with no change in cell viability

290    (Supplementary Fig. 11).  These results suggest that LCN-2 regulates Dab2-mediated

291    internalization of integrin β1, which is critical for cell adhesion and migration of IFNλ-exposed

292    neutrophils.

293

294

295

*AKT2 inhibitor reduces AMD-like phenotype in Cryba1 cKO mice*

297

298      We previously reported that AKT2 is an upstream regulator of NFκB-dependent LCN-2

299 gene expression[10]. Also, AKT2 can activate NFκB, which in turn is known to activate IFNλ and

300 its downstream genes[42,43]. Therefore, we next asked whether CCT128930, a potent and selective

301 inhibitor of AKT2[44], could block neutrophil infiltration into the retina by reducing the pro-

302 inflammatory signal in the diseased retina.  In the *Cryba1* cKO mice, the RPE is mildly

303 degenerated at 12 months of age, progressing to severe RPE degeneration with photoreceptor

304 degeneration by 20 months[16].  One year old *Cryba1* cKO mice injected intravitreally with

305 CCT128930 showed decreased expression of pAKT2, IFNλ and CXCL1 levels (Supplementary

306 Fig. 12) in the RPE/choroid compared to the vehicle control.  We also observed significantly

307 fewer neutrophils in the retinas of CCT128930 treated cKO mice relative to those given vehicle

308 only (Fig. 8a).  Importantly, CCT128930 also reversed the early RPE degeneration and reduced

309 the formation of deposits between Bruch's membrane and RPE (Fig. 8b-e).  We have previously

310 shown activation of Müller glia in our mouse model[10].  This condition, associated with reactive

311 gliosis, is critical for the onset of the inflammatory process in most retinal diseases[45-47].

312 Interestingly, CCT128930-treated *Cryba1* cKO mice also showed considerable restoration of

313 normal GFAP/CRALBP (Müller cell marker) staining relative to the vehicle-treated group (Fig.

314 8f).  It is plausible that these changes may be linked to the reduction in the pro-inflammatory

315 state in the retina of the CCT128930-treated cKO mice, as evident from decrease in neutrophil

316 infiltration (Fig. 8a) and pro-inflammatory mediators like IFNλ and CXCL1 (Supplementary Fig.

317 12).  As depicted in the schematic (Fig. 8g), our findings suggest that targeting the homing of

318    activated neutrophils into the retina by specifically inhibiting AKT2-driven inflammation is

319    potentially a novel therapeutic approach in early, dry AMD.

320

321

322

323

324

325

326

327

328

329

330

331

332

333

334

335

336

337

338

339

340

**Discussion**

AMD is one of the leading causes of blindness in the elderly and is an immense socio-economic burden on the aging population. The dry or atrophic form comprises about 90% of all AMD cases, and no definitive treatment or prevention is available for these patients[48]. To uncover the cellular and molecular mechanisms involved in immune system activation and regulation in AMD, we examined aspects of early, dry AMD in the following: human AMD patient samples, a mouse model with an early, dry AMD-like phenotype (the *Cryba1* cKO)[16], NOD-SCID immunodeficient mice and LCN-2^{-/-} mice. Using these tools, we show that IFNλ, a Type-III interferon, provides a signal for neutrophil homing into the retina during early AMD, by specifically upregulating LCN-2 in the neutrophils through the STAT1 pathway. We provide convincing evidence that LCN-2 regulates integrin β1-dependent neutrophil adhesion and transmigration. Increased expression of extracellular integrin β1 is known to increase cell adhesion, a requirement for increased transmigration of neutrophils[49]. We envisage that increased association between LCN-2 and Dab2 decreases integrin β1 internalization, which in turn increases the extracellular level of the integrin, activating transmigration into the retina and potentiating retinal degeneration.

Involvement of neutrophils in the pathogenesis of age-related diseases, such as Alzheimer's, and to some extent wet/neovascular AMD, has been previously reported[50,51]. In our previous study, we showed, for the first time, increased infiltration of LCN-2 positive neutrophils in the choroid and retina of early AMD patients compared to age-matched controls[10]. In addition to increased numbers of neutrophils in the retina, we found increased levels of activated

364    neutrophils in the peripheral blood of AMD patients compared to age-matched controls.

365    Increased IFNλ1 in the plasma and aqueous humor supports a scenario where IFNλ1 is

366    associated with increased activation of the surveilling neutrophils, possibly producing more

367    inflammatory factors and engaging a feed-forward loop that stimulates disease progression.

368    Since neutrophils typically have a short half-life, how do they contribute to AMD lesion

369    formation?  We suggest that chronic exposure to molecular triggers will repeatedly activate

370    surveilling neutrophils, and if this pattern persists over time, the repeated inflammatory insult

371    will contribute to tissue injury during AMD development.  The previous reports that human

372    neutrophils move into an activated state (CD66b^{high}) during inflammation and tissue infiltration

373    are consistent with such a scenario[52].

374

375        To further substantiate our premise that homing of neutrophils into the retina with

376    abnormal levels of LCN-2 potentiates outer retinal degeneration and aggravates RPE changes

377    characteristic of early atrophic AMD[53], we injected NOD-SCID immunodeficient mice with WT

378    and activated neutrophils.  As expected, the data clearly showed that IFNλ-exposed activated

379    neutrophils transmigrated into the retina and potentiated retinal degeneration.  However, WT

380    neutrophils or LCN-2$^{-/-}$ neutrophils that have lower levels of extracellular integrin β1, even after

381    IFNλ treatment, failed to cause such an effect, strongly suggesting that abnormal levels of LCN-

382    2 released from the infiltrating neutrophils trigger retinal degeneration.  These data clearly

383    corroborate our high-resolution RSCM imaging data illustrating the extravasation of large

384    numbers of IFNλ-activated wild type neutrophils into the retina.  The migration of neutrophils

385    from the circulation to the site of inflammation is very well recognized[54].  However, this is the

386    first report proposing a molecular mechanism directing the trafficking of neutrophils from the

17

387  systemic circulation into the eye that results in retinal injury.  Our findings suggest strongly that

388  such a mechanism contributes to AMD progression.  We believe that this process could be

389  specific to the early stages of the disease and therefore a potential target for the development of

390  novel treatments.

391

392      Taken together, we provide novel evidence that IFNλ triggers transmigration of

393  neutrophils into the retina through activation of the LCN-2/Dab2/integrin β1 signaling axis

394  leading to pathology in early AMD patients, as well as in a mouse model that mimics an early

395  AMD-like phenotype[16].  Further, our findings suggest that targeting activated neutrophils by

396  inhibiting AKT2 reduces neutrophil infiltration into the retina and reverses early AMD-like

397  phenotype changes.  We recognize that AKT2 inhibition can have other beneficial effects aside

398  from reducing neutrophil infiltration, such as reducing activation of Müller glia, which could

399  reduce or prevent AMD lesion formation.  While antioxidant micronutrients slow intermediate

400  AMD progression and anti-VEGF injections treat neovascular disease[55-57], no therapy is

401  available for the earliest stages of the disease.  Thus, AKT inhibitors should be assessed as

402  potential therapy at the earliest stages of AMD.  Several drugs targeting various isoforms of

403  AKT are currently in different phases of clinical trials[58,59].  However, accumulating reports

404  suggest adverse effects accompany treatment with AKT inhibitors.  Therefore, understanding the

405  consequences of localized inhibition *in vivo* as reported in this study might help to determine a

406  dose of the inhibitor that could be effective without the side-effects, in particular diarrhea,

407  hyperglycaemia and liver injuries, which have been observed in previous clinical trials of AKT

408  inhibitors[60-62].  In addition, since we have delineated the signaling axis that is activated in the

409  early stages of AMD, targeting individual components of this pathway may also be highly

410     beneficial for therapy. While we analyzed the entire NOD-SCID BABB-cleared mouse eye by

411     high-resolution RSCM, our data do not demonstrate the route of entry of the neutrophils into the

412     eye or the time course of their activation. We speculate that the red CMTPX dye-labeled

413     activated neutrophils transmigrate into the retina through the retinal capillaries that constitute the

414     blood-ocular barrier, however detailed knowledge of the route of entry and the number of

415     activated neutrophils transmigrating into the retina would provide a window of time for a better-

416     targeted therapy. Nevertheless, the present study provides a unique perspective to early, dry

417     AMD by identifying neutrophils as an important pathophysiologic cellular component in the

418     disease onset and progression. Hence, targeting neutrophils at the early stages of the disease is a

419     viable strategy for treating early, dry AMD.

420

421

422

423

424

425

426

427

428

429

430

431

432

**Methods**

**Antibodies**

PE/Cy7-tagged CD45 (Cat# 103114), APC-tagged Ly6C (cat# 128016), FITC-tagged CD66b (Cat# 555724), V450-tagged Ly6G (Cat# 560603), Alexa fluor 700-tagged CD11b (Cat# 557960) and Anti human CD34 antibody (Cat# 343602) were purchased from BD Biosciences, USA and PE-tagged IL-28AR antibody (Cat# 337804) was purchased from Biolegend, USA. Anti-Neutrophil Elastase (Cat# ab68672), anti-GRO alpha (CXCL1) (Cat# ab86436), anti-STAT1 (phosphor S727) (cat# ab109461), anti-IL28 receptor alpha or IL28R1 (Cat # ab224395), anti-Histone H3 citrunillated (Cat# ab219407), VCAM1 (Cat# ab134047), CD34 (Cat# 8158) and IL28 + IL29 (Cat# ab191426) antibodies were purchased from Abcam, USA.  Anti-ICAM-1 (Cat# SC-107), Anti-STAT1 (Cat# 9172T), anti-AKT (Cat# 4685S), anti-AKT2 (Cat# 2964S) and anti-DAB2 (Cat# 12906S) were purchased from Cell Signaling Technologies, USA.  Other antibodies used include: Alexa fluor 488-tagged β1 Integrin (Santa Cruz Biotechnology, USA; Cat# sc-374429 AF488), Anti-IL-28A/IFNλ2 (Antibodies online; Cat# ABIN357173), Anti-Ly6G (Antibodies online, USA; Cat ABIN1854937), IL-29 antibody (Biorbyt, USA; Cat# orb6201), anti-IFNα (Thermo Fisher, USA; Cat# 221001), anti-Myeloperoxidase/MPO (R&D Systems, USA; Cat# AF3667-SP), anti-LCN-2 (EMD Milipore; Cat# AB2267) and anti-Actin (Sigma Aldrich, USA; Cat# A2066).

**Animals**

βA3/A1-crystallin conditional knockout mice (*Cryba1* cKO) and LCN-2 KO mice were generated as previously explained[13,63]. NOD-SCID mice (NOD.CB17-Prkdescid/J; 4-5 weeks old) were purchased from The Jackson Laboratory, USA. All animal studies were conducted in accordance with the Guide for the Care and Use of Animals (National Academy Press) and were approved by the University of Pittsburgh Animal Care and Use Committee.

**Human Eyes**

The diagnosis and classification of AMD in human donor eyes was done as previously described[10]. For immunostaining, human donor eyes were obtained from the National Disease Research Interchange (NDRI; Philadelphia, Pennsylvania, USA) within 12–35 h of death. Donor eyes from 5 subjects with early, dry AMD (age range 79–95 years; mean age 85.8 years) and three aged controls (age range 77–89 years; mean age 82.5 years), with no evidence of macular disease were studied[10]. The study adhered to the norms of the Declaration for Helsinki regarding research involving human tissue. For immunophenotyping and soluble factors quantification experiments in human peripheral blood and aqueous humor, samples were collected from human donors, reporting to Narayana Nethralaya, Bangalore, India. All subjects underwent an ophthalmic exam, including visual acuity testing and retinal examination. Early AMD patients were diagnosed by fundus imaging, Amsler grid test and OCT imaging when deemed necessary and classified as per the AREDS[64]. Subjects with co-existing glaucoma or any other degenerative retinal disorders were excluded. The control group consisted of individuals without any history

479    of AMD, diabetes, cardiovascular disorders or retinal diseases. 4-6 mL blood samples were

480    collected in EDTA tubes from 18 controls and 43 AMD subjects by venipuncture. Aqueous

481    humor samples (~50 μL) were collected from subjects undergoing cataract surgery (n=7 control,

482    n=6 AMD) by anterior chamber paracentesis under sterile conditions. Within this group, early

483    AMD subjects, where surgery is not contra-indicated, were identified by the presence of drusen

484    and RPE abnormalities characterized by pigmentary changes in the retina in accordance with

485    AREDS classification. The demographic characteristics of the cohorts are described in Table S1.

486    All collected samples were immediately stored in a biorepository until further processing. All

487    patient samples and related clinical information were collected after obtaining approval by the

488    Narayana Nethralaya Institutional Review Board (IRB) and with written, informed consent from

489    patients.

490

491    **Immunostaining**

492

493    Freshly enucleated eyes were fixed in 2% paraformaldehyde (PFA) for 10 min and then

494    the anterior parts (cornea, lens, and attached iris pigmented epithelium) were removed. The

495    resulting posterior eyecups were fixed in 2% PFA for 1 h at room temperature either for

496    cryosections or RPE/ retina flat mount. For cryosections, the eyecups were dehydrated through

497    gradient sucrose solutions and embedded in OCT and for RPE/retina flat mounts, tissues were

498    removed after the eyecup was quartered like a petaloid structure. The resulting eyecup was

499    further cut radially into eight pieces from the optic nerve head to the periphery[17].

500    Immunostaining on human/mouse retina sections or on retina/RPE flatmounts were performed

501    by using appropriate primary antibody (1:100) and incubated at 4$^o$C overnight. The RPE/ retinal

502  flatmounts or human or mouse retina sections were washed with 1X TBS thrice and then stained

503  with appropriate secondary antibodies (1:300) with 1μg/mL DAPI (Sigma Aldrich,USA) in the

504  dark at room temperature for 2 h. The tissue sections or flatmounts were washed 6 times with 1X

505  TBS. The tissues were mounted on a cover slip with DAKO mounting agent and then visualized

506  under a confocal microscope (Zeiss LSM710, Switzerland)[10,17].

507

508  **Soluble factors quantification**

509  Peripheral venous blood was obtained by venipuncture (n=43 AMD patients and n=18

510  control subjects) and aqueous humor (AH) was collected by anterior chamber paracentesis in

511  AMD patients (n=6) and control subjects (n=7) from subjects undergoing cataract surgery.  The

512  levels of IFNα, IFNβ, IFNγ, IFNλ1-3, VEGF and CXCL1 were measured in plasma and AH by

513  bead-based multiplex ELISA (BioLegend, Inc, USA) using a flow cytometer (BD FACS Canto

514  II, FACS DIVA software, BD Biosciences, USA).  The absolute concentration for each analyte

515  was calculated based on the standard curve using LEGENDplex[TM] software (Biolegend, Inc,

516  USA).

517

518  **Immunophenotyping**

519

520  Cells from peripheral blood (n=43 AMD patients and n=18 control subjects) were labeled

521  using fluorochrome conjugated anti-human antibodies specific for leukocytes (CD45),

522  neutrophils (CD66b) and IFNλ receptor (IL-28R1) at room temperature for 45 minutes.  Red

523  blood cells from peripheral blood samples were lysed in 1X BD lysis buffer for 10 minutes,

524  washed and resuspended in 1X phosphate buffered saline prior to flow cytometry (BD FACS

525    Canto II, FACS DIVA software, BD Biosciences, USA) based acquisition and analysis.  Data

526    were analyzed using FCS Express 6 Flow Research Edition software.  The leukocyte populations

527    were identified by manual gating using SSC/CD45$^+$ profile.  Subsequent gating was done on

528    SSC/CD66b FITC to identify neutrophils.  The neutrophil activation status was determined based

529    on CD66b cell surface expression. CD45$^+$CD66b$^{high}$ cells were considered as activated

530    neutrophils and CD45$^+$CD66b$^{low}$ as inactive neutrophils. CD45$^+$CD66b$^{high/low}$ IL-28R1$^+$ indicated

531    IFNλ receptor positive neutrophils.  The percentage of positive cell events for each staining

532    panel was calculated.

533

534    **RPE isolation and culture**

535

536          Mouse RPE was isolated from control C57BL/6J mice (3 weeks old, n=9; Jackson

537    Laboratories, USA) and cultured by enucleating the eyes and then washed twice in DMEM

538    containing high glucose and incubated in 2% (weight/volume) Dispase (Roche, 10269638001) in

539    DMEM for 45 min at 37°C. The eyes were then washed twice in growth medium made of

540    DMEM (high glucose) containing 10% FCS, 1% penicillin/ streptomycin, 2.5 mM L-glutamine,

541    and 1X MEM nonessential amino acids (Gibco, Invitrogen, 11095). An incision was made

542    around the ora serrata of each eye and the anterior segment was removed. The resulting posterior

543    eyecups were placed in growth medium for 20 min at 37°C to initiate separation of the neural

544    retina from the RPE. The neural retina was removed and intact sheets of RPE cells were peeled

545    off the underlying Bruch's membrane and transferred in a sterile 60-mm culture dish, containing

546    fresh growth medium. The RPE sheets were washed thrice with growth medium and then twice

547    with calcium and magnesium free HBSS and then briefly triturated, using a fine point Pasteur

548     pipette. RPE cells were centrifuged at 200 g for 5 min and cultured in transwell plates in growth

549     medium[65].

550

551     **IFNλ overexpression in cultured RPE cells**

552

553             pLV-C-IL28A-GFPSpark and control vector were purchased from Sino Biological Inc.

554     (Beijing, China, Cat# MG51305-ACGLN). Primary mouse RPE cells (in a monolayer; 90%

555     confluent) were transfected with the respective vectors using X-tremeGENE transfection reagent

556     (Roche, Switzerland) following the manufacturer's instructions. The transfection efficiency was

557     estimated by evaluating the level of IL-28A/IFNλ released (into the cell-free supernatant) from

558     overexpression transfected RPE cells by ELISA, with respect to the control vector transfected

559     cells; a minimum of a three-fold increase in IL-28A/IFNλ level was considered appropriate for

560     performing further experiments with the conditioned media.

561

562     **Isolation and culture of neutrophils**

563

564             Neutrophils from WT and LCN-2$^{-/-}$ mice were isolated by centrifugation of bone marrow

565     cells, flushed from femurs and tibias and purified over a Percoll discontinuous density gradient

566     following isolation, neutrophils were resuspended at a density of 10 X 10$^6$ per ml in Ca$^{2+}$ and

567     Mg$^{2+}$ free HBSS, supplemented with 20 mM HEPES and then cultured in 37°C at a density of 3

568     X 10$^6$ cells per ml before stimulation with either recombinant IFNλ or conditioned media from

569     RPE cells overexpressing IFNλ[66,50].

570

**pHrodo phagocytic assay**

Neutrophils in culture were incubated with fluorescent-tagged particles (pHrodo™ Red E. coli BioParticles™ Conjugate for Phagocytosis assay kit, Thermo Fisher, USA, Cat# P35361) and flow cytometric evaluation of percentage cells which has engulfed the pHrodo particles (phagocytic cells) was performed by following the manufacturer's protocol.

**Integrin β1 shRNA transfection**

Integrin β1 shRNA lentiviral (Cat# sc-60044-V) and control shRNA (Cat# sc-108080) particles were purchased from Santa Cruz Biotechnology, USA. Mouse bone marrow derived neutrophils ($5 \times 10^6$ cells/mL in HBSS containing 20 mM HEPES) were plated and then transfected with integrin β1 shRNA lentiviral or control shRNA particles for 8 h, according to the manufacturer's protocol.

**Rapid neutrophil adhesion assay**

Mouse bone marrow derived neutrophils ($5 \times 10^6$ cells/mL in HBSS containing 20 mM HEPES) from LCN-2$^{-/-}$ mice and WT mice respectively or neutrophils transfected with either control shRNA or integrin β1 shRNA were subjected to rapid adhesion assay. Glass bottom 35 mm plates were coated for 16 h at 4°C with human fibrinogen (20 μg/well in endotoxin-free PBS). Neutrophils from all experimental conditions ($10^5$ per well; $5 \times 10^6$ per mL in 10% FCS, 1 mM CaCl2/MgCl2 in PBS, pH 7.2) were added, incubated for 10 min at 37°C, and then fixed on

594    ice in 1.5% glutaraldehyde for 60 min and then counted with computer assisted enumeration[50].

595

**Neutrophil transmigration assay**

597

598    Neutrophils ($5 \times 10^6$ cells/mL in HBSS containing 20 mM HEPES medium) from LCN-

599    2$^{-/-}$ and WT mice respectively or neutrophils transfected with either control shRNA or integrin

600    β1 shRNA were used to assess cell migration by using transwell plates[50]. Neutrophils were

601    plated on transwell inserts at 5 X $10^6$ cells per ml and then exposed to different experimental

602    conditions and cultured at 37°C. The cells at the bottom of the transwell were fixed with 1.5%

603    glutaraldehyde for 60 minutes, stained with Giemsa and then counted with computer assisted

604    enumeration[50].

605

**Estimation of percentage neutrophils in mouse retina**

607

608    Mouse retinas were dissected from enucleated eyes and digested with 0.05% collagenase

609    D (Roche, Switzerland, Cat# 11088858001) at 37°C for 30 min, teased with blunt end forceps

610    and pipetted to release cells, passed through a 70 μm cell strainer, and centrifuged at 1,300g, 4°C

611    for 20 minutes. The entire pellet was used for assessing the % neutrophils by flow cytometry,

612    after staining with anti-Ly6G, Ly6C, CD11b and CD45 antibodies at a concentration of 1 μg/mL

613    for 90 minutes at room temperature[67].

614

615

616

**Intracellular reactive oxygen species (ROS)**

     Flow cytometry was performed to evaluate the intracellular ROS in neutrophils by staining cells ($1 \times 10^6$ cells) from each experimental group with 2',7'–dichlorofluorescin diacetate (DCFDA, Sigma Aldrich, USA, Cat# D6883-50MG) (25 µg/ml) for 30 min at 37°C. Excess DCFDA was washed and cells were resuspended in PBS. The ROS content of the cells was measured on a flow cytometer[68].

**Estimation of intracellular and extracellular expression of integrin β1**

     Freshly cultured bone marrow-derived neutrophils from WT and LCN-2$^{-/-}$ mice were incubated with Alexa fluor 488-tagged β1-Integrin (Santa Cruz Biotechnology, USA) antibodies at a concentration of 1 µg/mL in PBS containing 1% BSA for 1 h and the cell surface expression of integrin β1 (FITC fluorescence) was evaluated among these cells as described previously[32]. For intracellular expression of integrin β1, cells were permeabilized with 0.1% Triton X-100 in PBS for 5 min at 25°C before incubating with anti-integrin β1 antibody at a concentration of 1 µg/mL in PBS containing 1% BSA for 1 h. Cell were analyzed by flow cytometry[68].

**SDS-PAGE and western blot analysis**

     SDS-PAGE and western blot analyses were performed by suspending and sonicating cells or tissue samples in RIPA lysis buffer (Millipore, Billerica, MA, 20-188) plus 1% protease and phosphatase inhibitors (Sigma)[17]. Samples were placed on ice for 20 min and then

640      centrifuged at 13,000 g for 20 min in 4$^o$C. The supernatants were subjected to protein estimation

641      by BCA kit (Thermo Fisher, USA). 12 μg of protein was used per sample and mixed with 4X

642      protein sample buffer (Invitrogen, Carlsbad, CA) with 5% 2-mercaptoethanol (Sigma Aldrich,

643      USA) and heated at 100°C for 10 min. Samples were loaded into a 4–12% Bis-Tris Nu-PAGE

644      gel (Invitrogen), electrophoresis was performed in MES buffer (Novex, Waltham, MA, USA).

645      Proteins were transferred to nitrocellulose membranes and blocked with 5% skim milk (Biorad,

646      USA) or 5% BSA (Sigma, for phosphorylated proteins)[17]. The primary antibodies were used at a

647      dilution of 1:1000 whereas, all secondary antibodies were used at a dilution of 1:3000.

648

**Preparation of recombinant lipocalin-2 (LCN-2) protein**

650

651         Full length LCN-2 cDNA was synthesized by GeneScipt, USA.  It was subcloned in

652      pET28a vector at NdeI and XhoI restriction site.  The construct was transformed into *E.coli*

653      DH5-α cells for amplification and *E.coli* Rosetta for expression. A single colony was grown

654      overnight as a mother culture. 10% of mother culture was inoculated and grown to 0.8-1.0 OD

655      and induced with 0.5 mM IPTG for 2 h at 37°C.  The cells were then pelleted by centrifugation

656      at 6000 rpm for 10 minutes at 4°C in a microfuge, resuspended in 10% volume of 20 mM Tris

657      pH 8.0, containing 300 mM NaCl and 10% Glycerol.  The mixture was sonicated for 30 seconds

658      on and off each for 6 cycles, and then centrifuged at 12000 rpm for 30 minutes at 4°C.  The

659      supernatant fraction was passed over a Nickel NTA (BioVision, USA) column as per the

660      manufacturer's protocol.  The column was washed twice with 10 times the bed volume with 20

661      mM Tris pH 8.0, with 300 mM NaCl, 10% Glycerol and 20 mM Imidazole.  The protein was

662      eluted with 20mM Tris pH 8.0, 300 mM NaCl, 10% Glycerol and 300 mM Imidazole with ~ 5

663     times the bed volume in multiple fractions.  The protein was polished over Sephacryl S-300 (GE

664     Healthcare, USA, GE17-0599-10) following overnight dialysis at 4°C in 1X PBS and 50%

665     Glycerol.  The filter (0.25 micron) sterilized protein was stored at -20°C in working aliquots.

666

667     **Protein-protein interaction**

668

669         The human proteome microarray 2.0 analysis was performed as a paid service from CDI

670     NextGen Proteomics, MD, USA.  Recombinant LCN-2 was analyzed for protein-protein

671     interaction profiling on the HuProtTM v3.1 human proteome array and the sample was probed

672     on array plates at 1 μg/mL, with data analyzed using GenePix software.  Hit identification was

673     assessed as the ratio of median value of the foreground to the median of the surrounding

674     background for each protein probe on the microarray, followed by normalization to the median

675     value of all neighboring probes within the 9x9x9 window size and represented as the significance

676     of the probe binding signal difference from random noise (Z-Score).  The cutoff Z-score was 6 in

677     this study for the triplicate analysis; only protein interactions with a Z-score above 6 were

678     considered[17].

679

680

681     **Enzyme-linked immunosorbent assay (ELISA)**

682
683         The RPE choroid complexes harvested from freshly enucleated mouse eyes were kept on

684     ice and then homogenized in 300 μL of complete extraction buffer (Abcam, USA, Cat#

685     ab193970).  The homogenized tissue was used to perform ELISA on 96-well microtiter plates

686     coated with tissue lysates and incubated overnight at 4°C. The plates were blocked with 5% BSA

687      for 2 h. After washing, 50 µl of appropriate primary antibody, diluted to 1:1000 was added to

688      each well and incubated for 2 h at room temperature. Bound cytokine was detected with

689      secondary IgG peroxidase (Sigma Aldrich, USA). The color was developed with TMB substrate

690      solution (BD Pharmingen, USA). The reaction was stopped with 2 N H2SO4 solution and

691      absorbance was measured at 450 nm using a microplate reader[69].

692

693      **Clearing and imaging of whole eyes**

694

695      Whole mouse eyes harvested from animals that had been injected with red CMTPX

696      labeled neutrophils were fixed overnight in 4% paraformaldehyde. As described previously[70,71],

697      eyes were subject to clearing by BA:BB through a series of PBS:Ethanol gradients to dehydrate

698      the organs prior to clearing with a 1:2 mixture of benzyl alcohol (Sigma, 305197) and benzyl

699      benzoate (Sigma, B6630). After the samples were visibly clear, they were mounted in BA:BB

700      solution between cover glass.

701

702      Each eye was scanned using the RS-G4 ribbon scanning confocal (Caliber ID) fitted with

703      a 20x/1.00 Glyc (CFI90 20XC, Nikon), correction collar set to 1.50. Linear interpolation of

704      561nm laser excitation (iChrome-MLE-LFA, Toptica) was set between 15-30% power, top to

705      bottom of z-stack. Emission was detected using a 630/69 band-pass filter, PMT settings were

706      HV, 85; offset, 5. Voxels measured (0.395 x 0.395 x 5.33µm). Each sample required

707      approximately 3.5 hours of total acquisition time. Imagery was collected at 16bit pixel depth and

708      comprised approximately 65GB per eye. Images were collected as ribbons and were stitched and

709      assembled using custom algorithms in MATLAB v2017b. Each dataset was converted to Nikon

710    ND2 format and deconvolved with a custom NIS-Elements application configured for the

711    Richardson-Lucy algorithm, line-scanning confocal, image noise level high and 0.76 μm pinhole.

712    The deconvolved images were then converted to IMS format and loaded in to Imaris 9.2.1

713    (Bitplane). Prior to any analysis in Imaris, a Gaussian Filter was applied with a filter width of

714    0.395.

715

716          Neutrophils were quantified using the spot count function in Imaris Surpass.  Spots were

717    quantified over the entire image and then manually edited to maintain only those spots that were

718    within the retina and Schlemm's canal.  Finally, all remaining spots were filtered by volume to

719    eliminate any structure that did not fall between 728-5800 $\mu m^3$ (11-22 μm diameter), an

720    approximate diameter of neutrophils, and to eliminate structures that were falsely selected during

721    spot counting.  Imaris surpass spot counting parameters were the same for all datasets: Enable

722    Region Growing = true; Estimated Diameter = 10.0 μm; Background Subtraction = true;

723    "Quality" above 190; Region Growing Type = Local Contrast; Region Growing Manual

724    Threshold = 139.744; Region Growing Diameter = Diameter From Volume.

725

726    **RNAseq analysis**

727

728          RPE-Choroid from enucleated eyes harvested from 5 and 10 month old *Cryba1*^{fl/fl} and

729    *Cryba1* cKO mice (n=4), respectively, were subjected to total RNA isolation as previously

730    described[66].  Approximately 30 ng/μL total RNA was used to perform RNA-sequencing as a paid

731    service from DNA Link, USA.  All sequence reads were mapped to the reference genome

732    (NCBI37/mm[9]) using the RNAseq mapping algorithm included in CLC Genomics Workbench.

733     The maximum number of mismatches allowed for the mapping was set at 2. To estimate gene

734     expression levels and analyze for differentially expressed genes among the different groups,

735     RPKM was calculated[72].

736

737     **Co-Immunoprecipitation**

738

739             To evaluate the association between LCN-2/Dab2 and also Dab2/integrin β1 in different

740     experimental conditions, cultured neutrophils from different experimental groups were subjected

741     to co-immunoprecipitation (Co-IP) using the Pierce™ Co-Immunoprecipitation Kit (Thermo

742     Fisher, USA, Cat# 26149). The cells were sonicated in IP Lysis/Wash Buffer (provided in the

743     kit) plus 1% protease inhibitors (Sigma Aldrich, USA). The total lysates were processed with the

744     kit according to the instructions. Seventy micrograms of lysates of each group were

745     immunoprecipitated with 10 μg immobilized LCN-2 and dab2 antibodies respectively at 4°C

746     overnight. Normal rabbit IgG (Santa Cruz, USA) was used as the negative control. After elution,

747     samples were loaded (15 μg per well) in SDS-PAGE and western blot was performed[17].

748

749     **Intravitreal injection of AKT2 inhibitor**

750

751             *Cryba1*^{fl/fl} and *Cryba1* cKO mice (Male, 12 months old; n=4) were intravitreally injected

752     with 2 μl inhibitor (500 μM of CCT128930 in 2.5% DMSO in PBS) or vehicle only (2.5%

753     DMSO in PBS) into the vitreous, once every week for three weeks.  All instruments were

754     sterilized with a steam autoclave.  Bacitracin ophthalmic ointment was applied postoperatively.

755     Animals were euthanized with $CO_2$ gas four weeks after the first injection and the retinas were

756    harvested for further study[10].

757

**Sub-retinal injection of neutrophils in NOD-SCID mice and OCT**

759

760    NOD-SCID mice (NOD.CB17-Prkdescid/J, Jackson Laboratories, USA, male, 4-5 weeks

761    old) were used for the study.  A large sample size, n=10, was taken to nullify any experimental

762    anomaly.  Mice were anaesthetized and sub-retinal injections of neutrophils from different

763    experimental groups or recombinant LCN-2 protein were given as described earlier[73].  Seven

764    days after treatment, the NOD-SCID mice were anaesthetized by intraperitoneal injection of a

765    ketamine and xylazine mixture and then subjected to Fundus imaging along with OCT analysis

766    using the Bioptigen Envisu R2210 system.  OCT images were analyzed on optical sections (100

767    sections per retina) from each eye ranging from -2.0 to +2.0 mm with respect to the optic nerve

768    head (ONH) using the FIJI-ImageJ (NIH) plugin provided with the instrument along with Diver

769    2.4 software (Bioptigen).  After the experiment, the animals were euthanized with $CO_2$ gas and

770    the eyes were harvested for further experiments.

771

**Hematoxylin-Eosin staining**

773

774    Eyes from NOD-SCID and AKT2 inhibitor-treated mice were fixed in 2.5%

775    glutaraldehyde followed by formalin, transferred to graded ethanol and dehydrated followed by

776    embeding in methyl methacrylate. Sections of 1 μm were cut and stained with hematoxylin and

777    eosin and observed under a light microscope[74].

778

**Quantification of sub-retinal deposits**

The number of drusen-like sub-retinal deposits were counted in a masked fashion from hematoxylin-eosin images of 12 month old *Cryba1*^{fl/fl}, vehicle-treated *Cryba1* cKO and AKT2 inhibitor treated *Cryba1* cKO mice retinae respectively. Quantification of drusen-like sub-retinal deposits were done from these images by using the ImageJ/NIH image analysis system in a masked fashion[75].

**Statistical analysis**

Statistical analysis was performed with Microsoft Excel and GraphPad Prism 6 software for Windows, using one-way ANOVA. Group means were compared using Tukey's post hoc test, with significance being set at $P < 0.05$. For experiments with human samples, comparisons between control and AMD groups were performed by Mann-Whitney test with significance being set at $p < 0.05$, the data distribution was determined by the Shapiro-Wilk normality test. Center lines and edge lines in box plot indicate medians and interquartile range, respectively and whiskers indicate the most extreme data points. The analyses were performed on triplicate technical replicates. Results are presented as mean ± standard deviation (SD)[76].

**Data availability**

All data generated or analysed during this study are included in this published article (and its Supplementary Information files).

## References

1. N. G. Lambert, H. ElShelmani, M. Singh, F. C. Mansergh, M. A. Wride, M. Padilla, D. Keegan, R. E. Hogg, B. K. Ambati, Risk factors and biomarkers of age-related macular degeneration. *Prog. Retin. Eye. Res.* **54**, 64-102 (2016).

2. J. W. Kinney, S. M. Bemiller, A. S. Murtishaw, A. M. Leisgang, A. M. Salazar, B. T. Lamb, Inflammation as a central mechanism in Alzheimer's disease. *Alzheimers Dement. (NY)*. **4**, 575-590 (2018).

3. K. U. Tufekci, R. Meuwissen, S Genc, K. Genc, Inflammation in Parkinson's disease. *Adv. Protein Chem. Struct. Biol*. **88**, 69-132 (2012).

4. J. Ambati, J. P. Atkinson, B. D. Gelfand, Immunology of age-related macular degeneration. *Nat. Rev. Immunol.* **13**, 438-451 (2013).

5. I. Akhtar-Schäfer, L. Wang, T. U. Krohne, H. Xu, T. Langmann, Modulation of three key innate immune pathways for the most common retinal degenerative diseases. *EMBO Mol. Med.* **10**, pii: e8259 (2018).

6. D. A. Copland, S. Theodoropoulou, J. Liu, A. D. Dick. A perspective of AMD through the eyes of immunology. *Invest. Ophthalmol. Vis. Sci.* **59**, AMD83-AMD92 (2018).

7. P. G. McMenamin, D. R. Saban, S. J. Dando, Immune cells in the retina and choroid: Two different tissue environments that require different defenses and surveillance. *Prog. Retin. Eye Res.* pii: S1350-9462(18)30058-2 (2018).

8. S. D. Kobayashi, F. R. DeLeo, Role of neutrophils in innate immunity: a systems biology-level approach. *Wiley Interdiscip. Rev. Syst. Biol. Med.* **1**, 309-333 (2009).

824    9.  C. Rosales, C.A. Lowell, M. Schnoor, E. Uribe-Querol, Neutrophils: their role in innate

825        and adaptive immunity. *J. Immunol. Res.* **2017**, 9748345 (2017).

826    10. S. Ghosh, P. Shang, M. Yazdankhah, I. Bhutto, S. Hose, S. R. Montezuma, T. Luo, S.

827        Chattopadhyay, J. Qian, G. A. Lutty, D. A. Ferrington, J. S. Zigler. Jr, D. Sinha,

828        Activating the AKT2-nuclear factor-κB-lipocalin-2 axis elicits an inflammatory response

829        in age-related macular degeneration. *J. Pathol.* **241**, 583-588 (2017).

830    11. M. Beyrau, J. V. Bodkin, S. Nourshargh, Neutrophil heterogeneity in health and disease:

831        a revitalized avenue in inflammation and immunity. *Open Biol*. **2**, 120134 (2012).

832    12. V. Abella, M. Scotece, J. Conde, R. Gómez, A. Lois, J. Pino, J. J. Gómez-Reino, F. Lago,

833        A. Mobasheri, O. Gualillo, The potential of lipocalin-2/NGAL as biomarker for

834        inflammatory and metabolic diseases. *Biomarkers* **20**, 565-71 (2015).

835    13. M. Valapala, M. Edwards, S. Hose, R. Grebe, I. A. Bhutto, M. Cano, T. Berger, T. W.

836        Mak, E. Wawrousek, J. T. Handa, G. A. Lutty, J. S. Zigler. Jr, D. Sinha, Increased

837        Lipocalin-2 in the retinal pigment epithelium of *Cryba1* cKO mice is associated with a

838        chronic inflammatory response. *Aging Cell* **13**,1091-4 (2014).

839    14. M. E. Pennesi, M. Neuringer, R. J. Courtney, Animal models of age related macular

840        degeneration. *Mol. Aspects Med*. **33**, 487-509 (2012).

841    15. P. Elizabeth Rakoczy, M. J. Yu, S. Nusinowitz, B. Chang, J. R. Heckenlively, Mouse

842        models of age-related macular degeneration. *Exp. Eye Res.* **82**, 741-52 (2006).

843    16. M. Valapala, C. Wilson, S. Hose, I. A. Bhutto, R. Grebe, A. Dong, S. Greenbaum, L. Gu,

844        S. Sengupta, M. Cano, S. Hackett, G. Xu, G. A. Lutty, L. Dong, Y. Sergeev, J. T. Handa,

845        P. Campochiaro, E. Wawrousek, J. S. Zigler. Jr, D. Sinha, Lysosomal-mediated waste

846        clearance in retinal pigment epithelial cells is regulated by CRYBA1/βA3/A1-crystallin

847        via V-ATPase-MTORC1 signaling. *Autophagy* **10**, 480-496 (2014).

848    17. P. Shang, M. Valapala, R. Grebe, S. Hose, S. Ghosh, I. A. Bhutto, J. T. Handa, G. A.

849        Lutty, L. Lu, J. Wan, J. Qian, Y. Sergeev, R. Puertollano, J. S. Zigler. Jr, G. T. Xu, D.

850        Sinha, The amino acid transporter SLC36A4 regulates the amino acid pool in retinal

851        pigmented epithelial cells and mediates the mechanistic target of rapamycin, complex 1

852        signaling. *Aging Cell* **16**, 349-359 (2017).

853    18. M. Wu, H. Zhang, C. Tie, C. Yan, Z. Deng, Q. Wan, X. Liu, F. Yan, H. Zheng, MR

854        imaging tracking of inflammation-activatable engineered neutrophils for targeted therapy

855        of surgically treated glioma. *Nat. Commun.* **9**, 4777 (2018).

856    19. R. K. Andrews, J. F. Arthur, E. E. Gardiner, Neutrophil extracellular traps (NETs) and

857        the role of platelets in infection. *Thromb. Haemost.* **112**, 659-65 (2014).

858    20. N. Gestermann, D. J. van der Windt, V. Sud, H. Zhang, P. R. Varley, J. Goswami, H. O.

859        Yazdani, S. Tohme, P. Loughran, R. M. O'Doherty, M. I. Minervini, H. Huang, R. L.

860        Simmons, A. Tsung, Netting neutrophils activate autoreactive B cells in lupus. *J.*

861        *Immunol.* **200**, 364-3371 (2018).

862    21. B. McDonald, R. P. Davis, S. J. Kim, M. Tse, C. T. Esmon, E. Kolaczkowska, C. N.

863        Jenne, Platelets and neutrophil extracellular traps collaborate to promote intravascular

864        coagulation during sepsis in mice. *Blood* **129**, 1357-1367 (2017).

865    22. D. J. van der Windt, V. Sud, H. Zhang, P. R. Varley, J. Goswami, H. O. Yazdani, S.

866        Tohme, P. Loughran, R. M. O'Doherty, M. I. Minervini, H. Huang, R. L. Simmons, A.

867        Tsung, Neutrophil extracellular traps promote inflammation and development of

868    hepatocellular carcinoma in nonalcoholic steatohepatitis. *Hepatology* **68**, 1347-1360

869    (2018).

870    23. J. D. Langereis, Neutrophil integrin affinity regulation in adhesion, migration, and

871    bacterial clearance. *Cell Adh. Migr.* **7**, 476-81 (2013).

872    24. L. Yang, R. M. Froio, T. E. Sciuto, A. M. Dvorak, R. Alon, F. W. Luscinskas, ICAM-1

873    regulates neutrophil adhesion and transcellular migration of TNF-alpha-activated

874    vascular endothelium under flow. *Blood* **106**, 584-592 (2005).

875    25. J. T. Kaifi, E. Diaconu, E. Pearlman, Distinct roles for PECAM-1, ICAM-1, and VCAM-

876    1 in recruitment of neutrophils and eosinophils to the cornea in ocular onchocerciasis

877    (river blindness). *J. Immunol.* **166**, 6795-801 (2001).

878    26. S. G. Maher, F. Sheikh, A. J. Scarzello, A. L. Romero-Weaver, D. P. Baker, R. P.

879    Donnelly, A. M. Gamero, IFNalpha and IFNlambda differ in their antiproliferative

880    effects and duration of JAK/STAT signaling activity. *Cancer Biol. Ther.* **7**, 1109-15

881    (2008).

882    27. S. Shao, T. Cao, L. Jin, B. Li, H. Fang, J. Zhang, Y. Zhang, J. Hu, G. Wang, Increased

883    Lipocalin-2 Contributes to the Pathogenesis of Psoriasis by Modulating Neutrophil

884    Chemotaxis and Cytokine Secretion. *J. Invest. Dermatol.* **136**, 1418-1428 (2016).

885    28. P. Zhao, J. M. Stephens, STAT1, NF-κB and ERKs play a role in the induction of

886    lipocalin-2 expression in adipocytes. *Mol. Metab.* **2**, 161-70 (2013).

887    29. V. Papayannopoulos, K. D. Metzler, A. Hakkim, A. Zychlinsky, Neutrophil elastase and

888    myeloperoxidase regulate the formation of neutrophil extracellular traps. *J. Cell. Biol.*

889    **191**, 677-91 (2010).

890   30. A. M. Watson, A. H. Rose, G. A. Gibson, C. L. Gardner, C. Sun, D. S. Reed, L. K. M.

891       Lam, C. M. St Croix, P. L. Strick, W. B. Klimstra, S. C. Watkins, Ribbon scanning

892       confocal for high-speed high-resolution volume imaging of brain. *PLoS. One* **12**,

893       e0180486 (2017).

894   31. Z. P. Du, B. L. Wu, Y. M. Xie, Y. L. Zhang, L. D. Liao, F. Zhou, J. J. Xie, F. M. Zeng,

895       X. E. Xu, W. K. Fang, E. M. Li, L. Y. Xu, Lipocalin 2 promotes the migration and

896       invasion of esophageal squamous cell carcinoma cells through a novel positive feedback

897       loop. *Biochim. Biophys. Acta*. **1853**, 2240-50 (2015).

898   32. A. Teckchandani, N. Toida, J. Goodchild, C. Henderson, J. Watts, B. Wollscheid, J. A.

899       Cooper, Quantitative proteomics identifies a Dab2/integrin module regulating cell

900       migration. *J. Cell Biol.* **186**, 99-111 (2009).

901   33. C. L. Huang, J. C. Cheng, C. H. Liao, A. Stern, J. T. Hsieh, C. H. Wang, H. L. Hsu, C. P.

902       Tseng, Disabled-2 is a negative regulator of integrin alpha(IIb)beta(3)-mediated

903       fibrinogen adhesion and cell signaling. *J. Biol. Chem.* **279**, 42279-89 (2004).

904   34. F. Rosenbauer, A. Kallies, M. Scheller, K. P. Knobeloch, C. O. Rock, M. Schwieger, C.

905       Stocking, I. Horak, Disabled-2 is transcriptionally regulated by ICSBP and augments

906       macrophage spreading and adhesion. *EMBO. J.* **21**, 211-20 (2002).

907   35. P. P. Sarangi, Y. M. Hyun, Y. V. Lerman, A. P. Pietropaoli, M. Kim, Role of β1 integrin

908       in tissue homing of neutrophils during sepsis. *Shock* **38**, 281-287 (2012).

909   36. S.D. Hanlon, C. W. Smith, M. N. Sauter, A. R. Burns, Integrin-dependent neutrophil

910       migration in the injured mouse cornea. *Exp. Eye Res.* **120**, 61-70 (2014).

911   37. A. Schroll, K. Eller, C. Feistritzer, M. Nairz, T. Sonnweber, P.A. Moser, A. R.

912       Rosenkranz, I. Theurl, G. Weiss, Lipocalin-2 ameliorates granulocyte functionality. *Eur.*

913    *J. Immunol*. **42**, 3346-57 (2012).

914    38. Y. V. Lerman, K. Lim, Y. M. Hyun, K. L. Falkner, H, Yang, A. P. Pietropaoli, A.

915    Sonnenberg, P. P. Sarangi, M. Kim, Sepsis lethality via exacerbated tissue infiltration and

916    TLR-induced cytokine production by neutrophils is integrin α3β1-dependent. *Blood* **124**,

917    3515-23 (2004).

918    39. M. Scholz, P. Nowak, A. Schuller, S. Margraf, R. Blaheta, J. Cinatl, J. Windolf, A.

919    Moritz, Cardiac surgery with extracorporeal circulation: neutrophil transendothelial

920    migration is mediated by beta1 integrin (CD29) in the presence of TNF-alpha. *J. Invest.*

921    *Surg*. **17**, 239-47 (2004).

922    40. P. Subramanian, I. Mitroulis, G. Hajishengallis, T. Chavakis, Regulation of tissue

923    infiltration by neutrophils: role of integrin α3β1 and other factors. *Curr. Opin. Hematol*.

924    **23**, 36-43.

925    41. M. R. Cera, M. Fabbri, C. Molendini, M. Corada, F. Orsenigo, M. Rehberg, C. A.

926    Reichel, F. Krombach, R. Pardi, E. Dejana, JAM-A promotes neutrophil chemotaxis by

927    controlling integrin internalization and recycling. *J. Cell. Sci.* **122**, 268-77 (2009).

928    42. Y. Gao, R. B. Gartenhaus, R. G. Lapidus, A. Hussain, Y. Zhang, X. Wang, H. C. Dan,

929    Differential IKK/NF-κB Activity Is Mediated by TSC2 through mTORC1 in PTEN-Null

930    Prostate Cancer and Tuberous Sclerosis Complex Tumor Cells. *Mol. Cancer Res.* **13**,

931    1602-14 (2015).

932    43. A. A. Price, D. Tedesco, M. R. Prasad, K. A. Workowski, C. M. Walker, M. S. Suthar, J.

933    R. Honegger, Grakoui A, Prolonged activation of innate antiviral gene signature after

934    childbirth is determined by IFNL3 genotype. *Proc. Natl. Acad. Sci. U.S.A.* **113**, 10678-83

935    (2016).

936     44. T. A. Yap, M. I. Walton, L. J. Hunter, M. Valenti, A. de Haven Brandon, P. D. Eve, R.

937         Ruddle, S. P. Heaton, A. Henley, L. Pickard, G. Vijayaraghavan, J. J. Caldwell, N. T.

938         Thompson, W. Aherne, F. I. Raynaud, S. A. Eccles, P. Workman, I. Collins, M. D.

939         Garrett, Preclinical pharmacology, antitumor activity, and development of

940         pharmacodynamic markers for the novel, potent AKT inhibitor CCT128930. *Mol. Cancer*

941         *Ther.* **10**, 360-371 (2011).

942     45. C. Hippert, A. B. Graca, A. C. Barber, E. L. West, A. J. Smith, R. R. Ali, R. A. Pearson,

943         Müller glia activation in response to inherited retinal degeneration is highly varied and

944         disease-specific. *PLoS One* **10**, e0120415 (2015).

945     46. D. M. Inman, P. J. Horner, Reactive nonproliferative gliosis predominates in a chronic

946         mouse model of glaucoma. *Glia* 55, 942-53 (2007).

947     47. K. H. Wu, M. C. Madigan, F. A. Billson, P. L. Penfold, Differential expression of GFAP

948         in early v late AMD: a quantitative analysis. *Br. J. Ophthalmol.* **87**, 1159-66 (2003).

949     48. J. Köberlein, K. Beifus, C. Schaffert, R. P. Finger, The economic burden of visual

950         impairment and blindness: a systematic review. *B. M. J. Open* **3**, e003471 (2013).

951     49. R. I. Clyman, F. Mauray, R. H. Kramer, Beta 1 and beta 3 integrins have different roles

952         in the adhesion and migration of vascular smooth muscle cells on extracellular matrix.

953         *Exp. Cell Res*. **200**, 272-84 (1992).

954     50. E. Zenaro, E. Pietronigro, V. Della Bianca, G. Piacentino, L. Marongiu, S. Budui, E.

955         Turano, B. Rossi, S. Angiari, S. Dusi, A. Montresor, T. Carlucci, S. Nanì, G. Tosadori, L.

956         Calciano, D. Catalucci, G. Berton, B. Bonetti, G. Constantin, Neutrophils promote

957         Alzheimer's disease-like pathology and cognitive decline via LFA-1 integrin. *Nat. Med.*

958         **21**, 880-6 (2015).

959     51. M. Krogh Nielsen, S. M. Hector, K. Allen, Y. Subhi, T. L. Sørensen, Altered activation

960         state of circulating neutrophils in patients with neovascular age-related macular

961         degeneration. *Immun. Ageing* **14**, 18 (2017).

962     52. E. Fortunati, K. M. Kazemier, J. C. Grutters, L. Koenderman, V. J. Van den Bosch,

963         Human neutrophils switch to an activated phenotype after homing to the lung irrespective

964         of inflammatory disease. *Clin. Exp. Immunol.* **155**, 559-66 (2009).

965     53. X. Ding, M. Patel, C. C. Chan, Molecular pathology of age-related macular degeneration.

966         *Prog. Retin. Eye Res.* **28**, 1-18 (2009).

967     54. Rosales C, Neutrophil: A Cell with Many Roles in Inflammation or Several Cell Types?

968         *Front. Physiol*. **9**, 113 (2018).

969     55. Age-Related Eye Disease Study Research Group, A randomized, placebo-controlled,

970         clinical trial of high-dose supplementation with vitamins C and E, beta carotene, and zinc

971         for age-related macular degeneration and vision loss: AREDS report no. 8. *Arch.*

972         *Ophthalmol.* **126**, 1251 (2008).

973     56. E. Y. Chew, T. E. Clemons, E. Agrón, R. D. Sperduto, J. P. Sangiovanni, N. Kurinij, M.

974         D. Davis, Long-term effects of vitamins C and E, β-carotene, and zinc on age-related

975         macular degeneration: AREDS report no. 35. *Ophthalmology* **120**, 1604-11.e4 (2013) .

976     57. C. L. Nguyen, L. J. Oh, E. Wong, J. Wei, M. Chilov, Anti-vascular endothelial growth

977         factor for neovascular age-related macular degeneration: a meta-analysis of randomized

978         controlled trials. *B. M. C. Ophthalmol.* **18**, 130 (2018).

979     58. C. X. Ma, V. Suman, M. P. Goetz, D. Northfelt, M. E. Burkard, F. Ademuyiwa, M.

980         Naughton, J. Margenthaler, R. Aft, R. Gray, A. Tevaarwerk, L. Wilke, T. Haddad, T.

981         Moynihan, C. Loprinzi, T. Hieken, E. K. Barnell, Z. L. Skidmore, Y. Y. Feng, K.

Krysiak, J. Hoog, Z. Guo, L. Nehring, K. B. Wisinski, E. Mardis, I. S. Hagemann, K. Vij, S. Sanati, H. Al-Kateb, O. L. Griffith, M. Griffith, L. Doyle, C. Erlichman, M. J. Ellis, A Phase II Trial of Neoadjuvant MK-2206, an AKT Inhibitor, with Anastrozole in Clinical Stage II or III PIK3CA-Mutant ER-Positive and HER2-Negative Breast Cancer. *Clin. Cancer Res*. **23**, 6823-6832 (2017).

59. LOTUS investigators, Ipatasertib plus paclitaxel versus placebo plus paclitaxel as first-line therapy for metastatic triple-negative breast cancer (LOTUS): a multicentre, randomised, double-blind, placebo-controlled, phase 2 trial. *Lancet Oncol*. **10**, 1360-1372 (2017).

60. B. D. Manning, A. Toker, AKT/PKB Signaling: Navigating the Network. *Cell* **169**, 381-405 (2017).

61. J. S. Brown, U. Banerji, Maximising the potential of AKT inhibitors as anti-cancer treatments. *Pharmacol. Ther*. **172**, 101-115 (2017).

62. Q. Wang, X. Chen, N. Hay, Akt as a target for cancer therapy: more is not always better (lessons from studies in mice). *Br. J. Cancer* **117**, 159-163 (2017).

63. T. Berger, A. Togawa, G. S. Duncan, A. J. Elia, A. You-Ten, A. Wakeham, H. E. Fong, C. C. Cheung, T. W. Mak, Lipocalin 2-deficient mice exhibit increased sensitivity to Escherichia coli infection but not to ischemia-reperfusion injury. *Proc. Natl. Acad. Sci. U. S. A*. **103**, 1834-9 (2006).

64. Age-Related Eye Disease Study Research Group. The Age-Related Eye Disease Study system for classifying age-related macular degeneration from stereoscopic color fundus photographs: the Age-Related Eye Disease Study Report Number 6. *Am. J. Ophthalmol*. 132, 668-81 (2001).

65. P. Shang, N. A. Stepicheva, S. Hose, J. S. Zigler. Jr, JS, D. Sinha, Primary Cell Cultures from the Mouse Retinal Pigment Epithelium. *J. Vis. Exp*. **133**, e56997 (2018).

66. A. Broggi, Y. Tan, F. Granucci, I. Zanoni, IFN-λ suppresses intestinal inflammation by non-translational regulation of neutrophil function. *Nat. Immunol.* **18**, 1084-1093 (2017).

67. Z. Zhao, Y. Liang, Y. Liu, P. Xu, M. J. Flamme-Wiese, D. Sun, J. Sun, R. F. Mullins, Y. Chen, J. Cai, Choroidal γδ T cells in protection against retinal pigment epithelium and retinal injury. *FASEB. J.* **31**, 4903-49 (2017).

68. S. Ghosh, S. Mukherjee, S. Choudhury, P. Gupta, A. Adhikary, R. Baral, S. Chattopadhyay, Reactive oxygen species in the tumor niche triggers altered activation of macrophages and immunosuppression: Role of fluoxetine. *Cell Signal*. **27**, 1398-412 (2015).

69. S. Roy, K. Lu, M. K. Nayak, A Bhuniya, T. Ghosh, S. Kundu, S. Ghosh, R Baral, P. S. Dasgupta, S. Basu, Activation of D2 Dopamine Receptors in CD133+ve Cancer Stem Cells in Non-small Cell Lung Carcinoma Inhibits Proliferation, Clonogenic Ability, and Invasiveness of These Cells. *J. Biol. Chem.* **292**, 435–445 (2017).

70. S. Waxman, R. T. Loewen, Y. Dang, S. C. Watkins, A. M. Watson, N. A. Loewen, High-Resolution, Three-Dimensional Reconstruction of the Outflow Tract Demonstrates Segmental Differences in Cleared Eyes. *Invest. Ophthalmol. Vis. Sci*. **59**, 2371-2380 (2018).

71. H. U. Dodt, U. Leischner, A. Schierloh, N. Jährling, C. P. Mauch, K. Deininger, J. M. Deussing, M. Eder, W. Zieglgänsberger, K. Becker, Ultramicroscopy: three-dimensional visualization of neuronal networks in the whole mouse brain. *Nat. Methods* **4**, 331-6 (2007).

72. A. Mortazavi, B. A. Williams, K. McCue, L. Schaeffer, B. Wold, Mapping and quantifying mammalian transcriptomes by RNA-Seq. *Nat. Methods* **5**: 621–628 (2008).

73. J. Maruotti, S. R. Sripathi, K. Bharti, J. Fuller, K. J. Wahlin, V. Ranganathan, V. M. Sluch, C. A. Berlinicke, J. Davis, C. Kim, L. Zhao, J. Wan, J. Qian, B. S. R. Corneo. B. Dubey, Z. Olenyuk, I. Bhutto, G. A. Lutty, D. J. Zack, Small-molecule-directed, efficient generation of retinal pigment epithelium from human pluripotent stem cells. *Proc. Natl. Acad. Sci. U. S. A.* **112**, 10950-5 (2015).

74. D. Sinha, S. Hose, C. Zhang, R. Neal, M. Ghosh, T. P. O'Brien, O. Sundin, M. F. Goldberg, W. G. Robison. Jr, P. Russell, W. K. Lo, J. S. Zigler. Jr, A spontaneous mutation affects programmed cell death during development of the rat eye. *Exp. Eye. Res.* **80**, 323–335 (2005).

75. T. Prasad, P. Zhu, A. Verma, P. Chakrabarty, A. M. Rosario, T. E. Golde, Q. Li, Amyloid β peptides overexpression in retinal pigment epithelial cells via AAV-mediated gene transfer mimics AMD-like pathology in mice. *Sci. Rep*. **7**, 3222 (2017).

76. S. Ghosh, P. Shang, H. Terasaki, N. Stepicheva, S. Hose, M. Yazdankhah, J. Weiss, T. Sakamoto, I. A. Bhutto, S. Xia, J. S. Zigler. Jr, R. Kannan, J. Qian, J. T. Handa, D. Sinha, A Role for βA3/A1-Crystallin in Type 2 EMT of RPE Cells Occurring in Dry Age-Related Macular Degeneration. *Invest. Ophthalmol. Vis. Sci*. **59**, AMD104-AMD113 (2018).

**Author contributions**

DS designed the study. SG, AP, TV, AW, IB, SH, PS, NS, MY, JW, MD conducted the experiments. SG, AW, IB, MD, AJ, SZ, SS, TB, TM, JTH, SW, AG, DS analyzed the data. SG, AP, TV, IB, SG, A, NY, SX, JQ, GL, SS, AG contributed to the human studies. SG, AW, SH, SZ, SS, JTH, AG, DS wrote the paper.

**Competing interests**

AJ is an employee of F. Hoffmann-La Roche, Ltd., Basel, Switzerland. AJ and DS are inventors in a US patent filed by F. Hoffmann-La Roche, Ltd., Basel, Switzerland.

1074
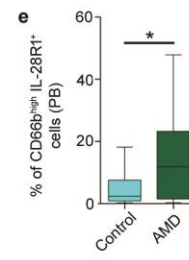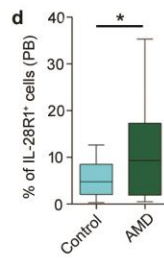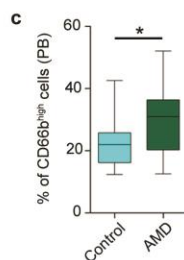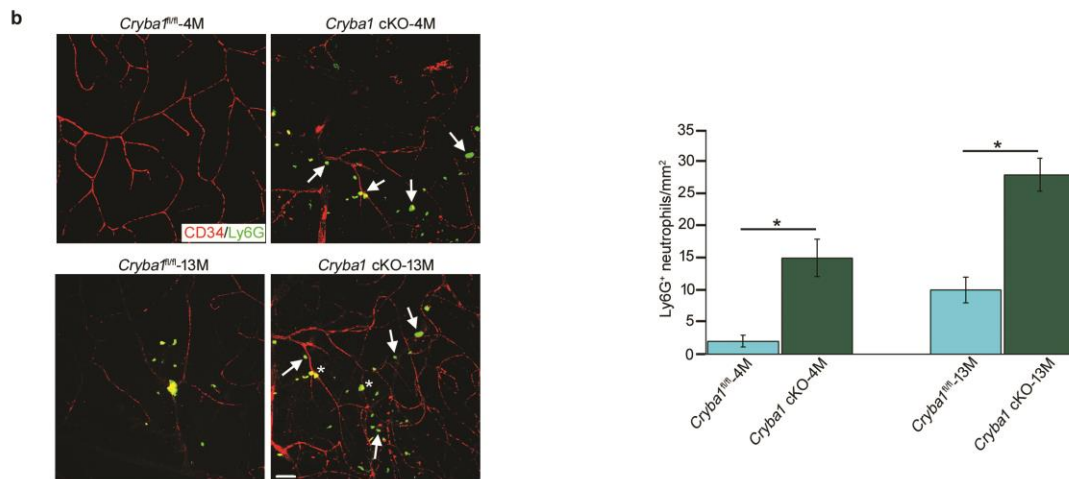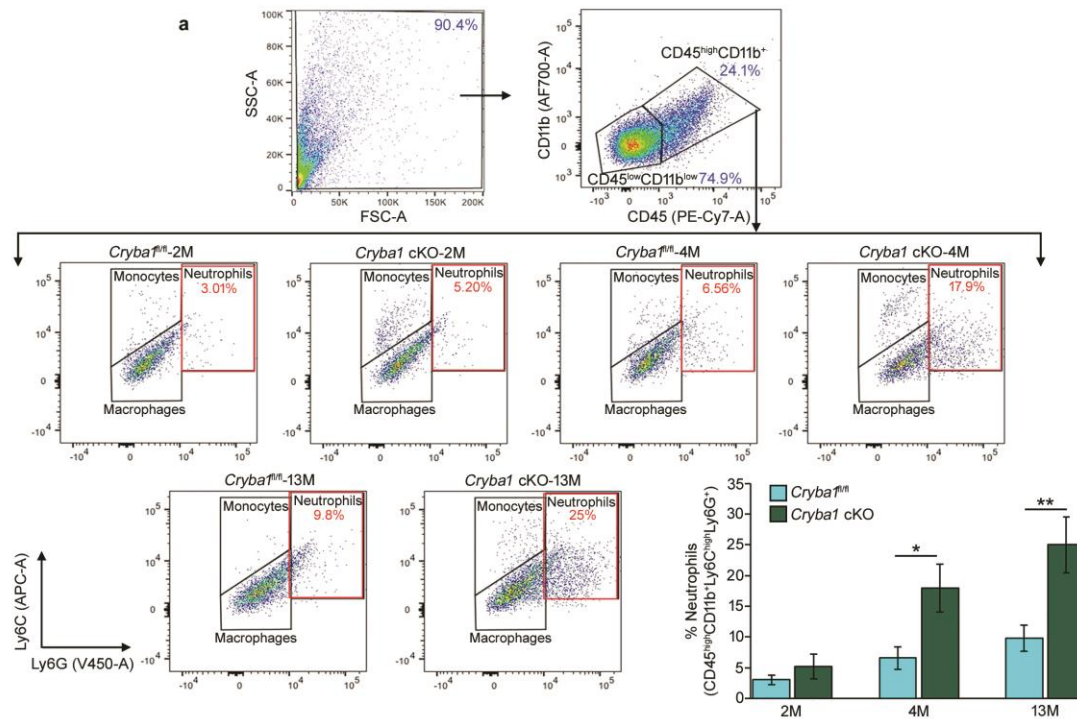
**Fig. 1. Neutrophil accumulate into the retina of *Cryba1* cKO mice and in peripheral blood**

**of human early AMD patients**. (**a**) Representative dot plots are gated on the CD45⁺CD11b⁺

1077 cells from mice retina. The total population of $CD45^+CD11b^+$ cells is considered to be 100%,

1078 with $CD45^{high}CD11b^+$ (neutrophils, monocytes, and macrophages) and $CD45^{low}CD11b^+$

1079 (predominantly resident microglia) gated separately (arrows denoting population lineages). The

1080 level of Ly6C and Ly6G on the $CD45^{high}CD11b^+$ population was assessed to evaluate %

1081 neutrophils (%$CD45^{high}CD11b^+Ly6C^{high}Ly6G^+$ cells), which showed increased neutrophils only

1082 in 4 and 13 month old *Cryba1* cKO mouse retinas compared to aged-matched controls

1083 (*Cryba1*$^{fl/fl}$). No differences were observed between *Cryba1*$^{fl/fl}$ and cKO retinas at 2 months of

1084 age. n=4. *$P< 0.05$ and **$P< 0.01$ (one-way ANOVA and Tukey's post-hoc test). (**b**)

1085 Immunofluorescence studies and quantification of Ly6G$^+$ cells (Green, Neutrophil marker) on

1086 retinal flatmounts, counterstained with CD34 (Red, marker for endothelial cells of blood vessels)

1087 revealed that neutrophils accumulated progressively in *Cryba1* cKO mouse retina (white arrows)

1088 and along the retinal blood vessels (yellow, asterisk), relative to age-matched control

1089 (*Cryba1*$^{fl/fl}$). n=4. *$P< 0.05$ (one-way ANOVA and Tukey's post-hoc test). Scale bar, 50 μm. In

1090 early AMD patients, flow cytometry data revealed significant increase in the peripheral blood

1091 (PB) levels of (**c**) total neutrophils (CD66b$^+$ cells), (**d**) total IL28R1$^+$ cells and (**e**) IL28R1$^+$

1092 expressing activated neutrophils (CD66b$^{high}$IL28R1$^+$). PB (AMD; n=43 and Controls; n=18).

1093 *$P< 0.05$ (Mann-Whitney test).

1094

1095

1096

1097

1098

1099
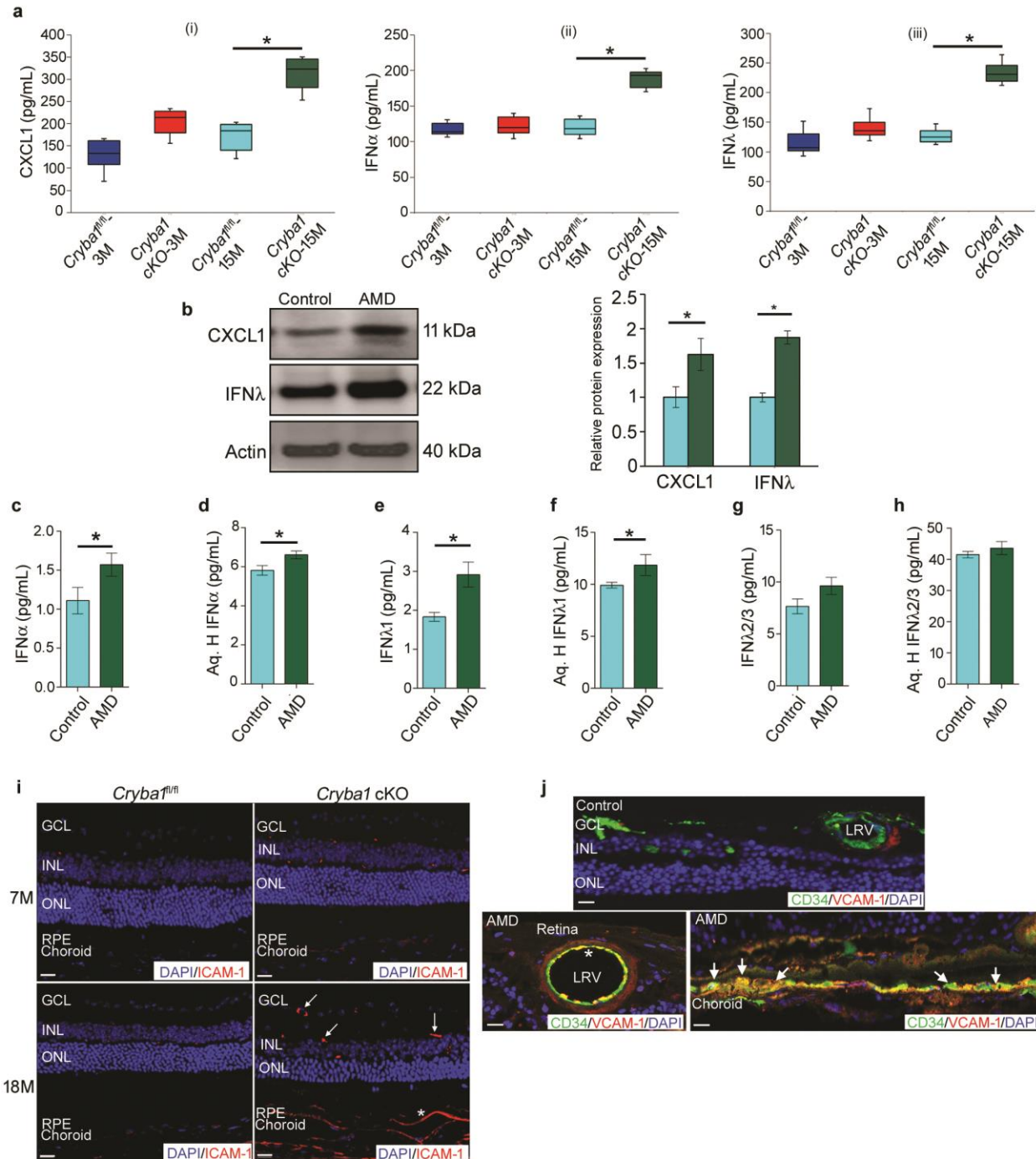
1100

**Fig. 2. Increased levels of neutrophil regulating factors in retinas from *Cryba1* cKO mice and human early AMD donor eyes.** (**a**) The levels of (**i**) CXCL1, (**ii**) IFNα and (**iii**) IFNλ were increased in the RPE-choroid tissue homogenate of 15 month old *Cryba1* cKO mice compared to age-matched *Cryba1*^fl/fl controls as measured by ELISA. No changes were observed in 3 month

1105 old mice. n=4. *$P < 0.05$ (one-way ANOVA and Tukey's post-hoc test). (**b**) Representative

1106 immunoblot and densitometry showed elevated CXCL1 and IFNλ in RPE lysates from early

1107 AMD donor samples compared to age- matched controls. n=6. *$P < 0.05$ (one-way ANOVA and

1108 Tukey's post-hoc test). (**c-h**) Multiplex ELISA revealed significant increases in the levels of

1109 IFNα and IFNλ1 in plasma or aqueous humor (AH) of early AMD patients relative to controls.

1110 No noticeable change was observed in the plasma and AH levels of IFNλ2/3. Plasma (AMD;

1111 n=43 and Controls; n=18), AH (AMD; n=6 and Controls; n=7). *$P < 0.05$ (Mann-Whitney test).

1112 (**i**) Immunofluorescence assay showing increased staining of ICAM-1 (Red, neutrophil adhesion

1113 molecule) in the neural retina (white arrows) and RPE/choroid (asterisk) of aged (18 month old)

1114 *Cryba1* cKO mice compared to age-matched control. No significant increase in staining was

1115 observed in the retina of 7 month old *Cryba1* cKO mice. n=5. Scale bar, 50 μm. (**j**)

1116 Immunostaining of human early AMD sections revealed increased staining of VCAM-1 (Red,

1117 neutrophil adhesion marker) in the large retinal vessels (LRV, asterisk), which were stained with

1118 CD34 (Green, marker for endothelial cells of blood vessels). Intense staining was also observed

1119 in the RPE/choroid (Yellow, white arrows). No noticeable staining for VCAM-1 was observed in

1120 the control sections. n=5. Scale bar, 50 μm.

1121

1122

1123

1124

1125

1126

1127
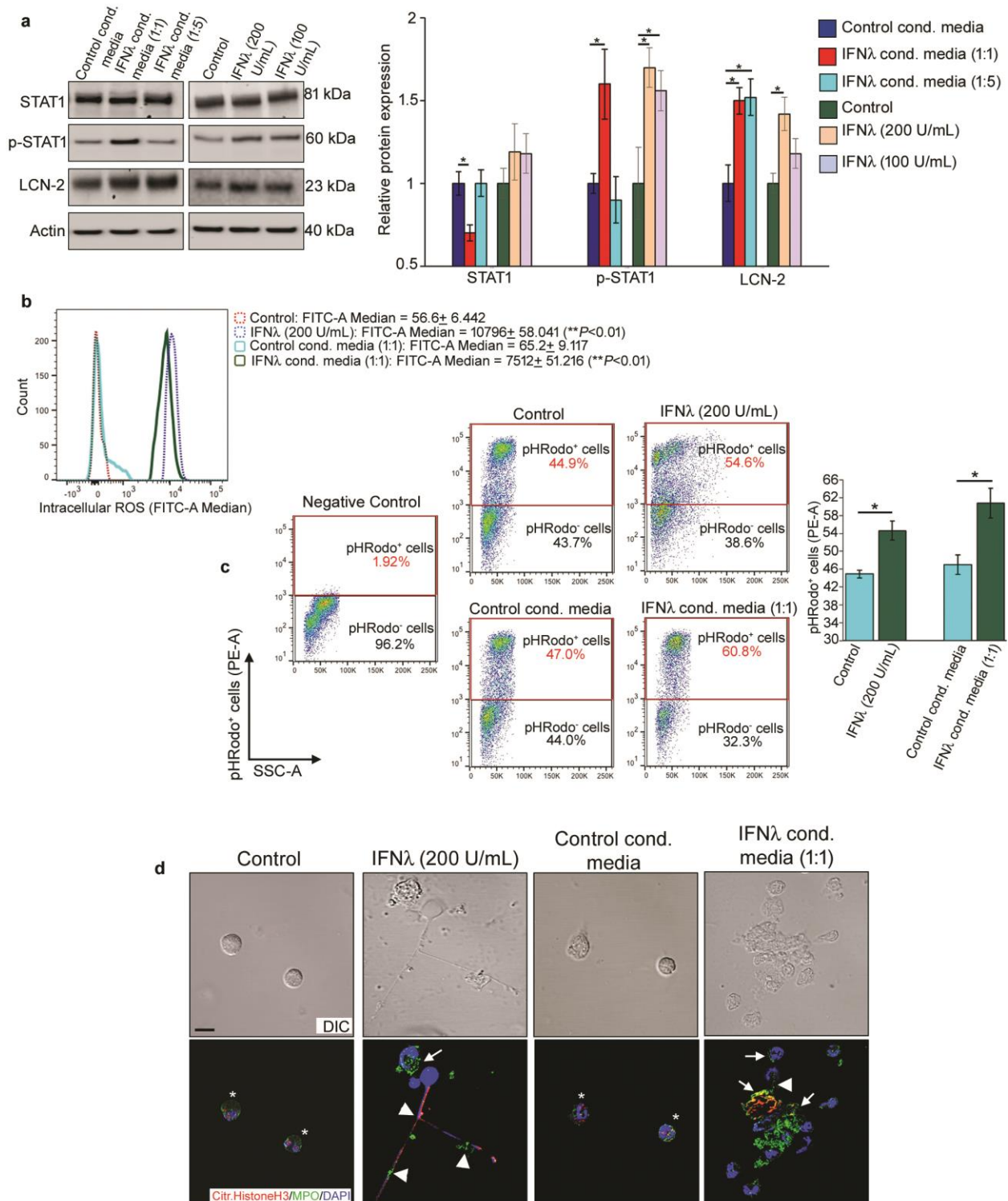
1128

**Fig. 3. IFNλ triggers LCN-2 upregulation and activation in neutrophils.** (**a**) Neutrophils

exposed to conditioned media from IFNλ overexpressing RPE cells (for 6 h) or to recombinant

1131    IFNλ (for 2 h), showed increased expression of LCN-2 and p-STAT1 compared to control cells.

1132    IFNλ conditioned media (1:1) and recombinant IFNλ (200 U/mL) were used as the effective

1133    dose in other experiments, since they showed maximum effect in terms of LCN-2 upregulation.

1134    n=4. *$P$< 0.05 (one-way ANOVA and Tukey's post-hoc test). (**b**) Flow cytometric evaluation of

1135    intracellular ROS was performed by staining neutrophils from culture (as described in **a**) with

1136    2',7' –dichlorofluorescein diacetate (DCFDA). ROS levels was represented by fluorescence

1137    intensity (FITC-A Median) values for 2',7'-dichlorofluorescein, (DCF, oxidized DCFDA),

1138    which showed significant increase in ROS levels among IFNλ-exposed neutrophils with respect

1139    to control. n=4. **$P$< 0.01, with respect to control (one-way ANOVA and Tukey's post-hoc

1140    test). (**c**) Phagocytosis assay was performed using pHRodo fluorescent labelled *E. coli.* particles

1141    in cultured neutrophils (as described in **a**). Flow cytometry analysis, upon gating on the negative

1142    control revealed, increased population of cells (red gating box), that have phagocytosed pHRodo

1143    *E. coli* conjugates among the IFNλ-exposed neutrophils groups relative to controls. n=4.  *$P$<

1144    0.05 (one-way ANOVA and Tukey's post-hoc test). (**d**) Neutrophil extracellular traps (NETs)

1145    were evaluated by staining cultured neutrophils (as described in **a**) with citrullinated histone H3

1146    (Citr. Histone H3, Red) and myeloperoxidase (MPO, Green) antibodies. Increased double

1147    staining for NETs, which are extracellular nuclear material (DAPI, Blue), with MPO (Yellow,

1148    arrow heads) or with citrullinated histone H3 (Magenta, arrow heads) were observed in IFNλ-

1149    treated neutrophils. This was concomitant with increased cellular expression of MPO (arrow) in

1150    these cells.  Controls did not show any extracellular nuclear material or NETs (asterisks). n=3.

1151    Scale bar, 50 μm.

1152

1153
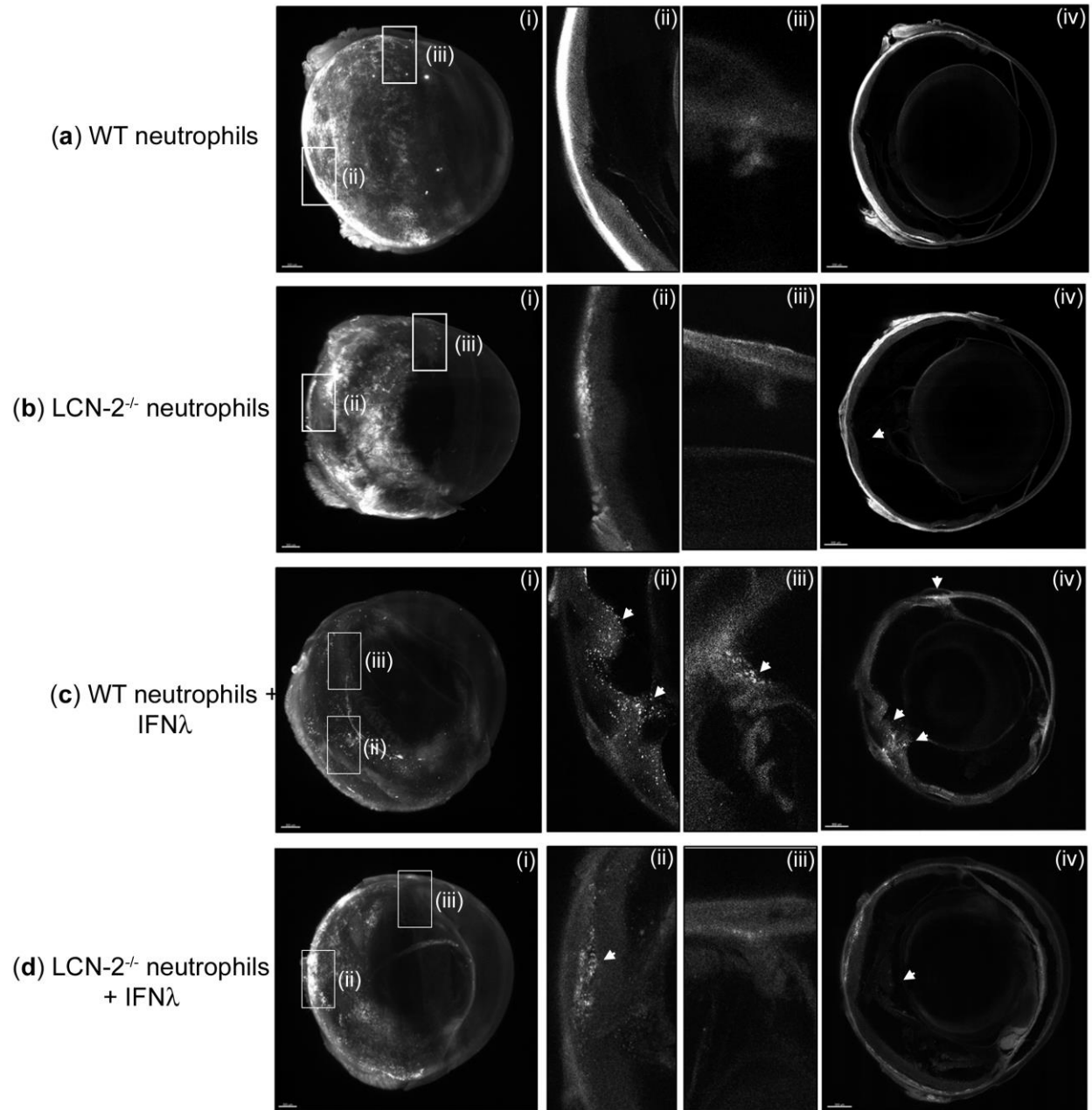
**Fig. 4. IFNλ triggers neutrophil homing into the eye *in vivo*.** Ribbon scanning confocal

microscopy (RSCM) was used to image neutrophil infiltration into whole cleared eyes from

NOD-SCID mice intravenously injected with; untreated (**a**) WT and (**b**) LCN-2^{-/-} neutrophils or

IFNλ-exposed (200 U/mL), (**c**) WT or (**d**) LCN-2^{-/-} neutrophils, tagged with red CMTPX. (**i**) 3D

1159     volumetric and (**iv**) orthogonal projections from whole eyes obtained from mice injected with,

1160     (**a**) WT neutrophils, did not show neutrophil homing (**ii**) into the retina or

1161     (**iii**) in through the aqueous humor drainage route (Schlemm's canal, a channel at the limbus and

1162     forms the joining point between the cornea and sclera, encircling the cornea). (**b**) Mice injected

1163     with LCN-2$^{-/-}$ neutrophils showed (**iv**) prevalence of neutrophils in the eye (arrow), but no

1164     infiltration was noticed into the (**ii**) retina or (**iii**) Schlemm's canal. (**c**) Mice injected with IFNλ-

1165     treated WT neutrophils showed noticeable infiltration of neutrophils into the (**i** and **iv**) eye

1166     (arrows), particularly in the (**ii**) retina (arrow) and (**iii**) Schlemm's canal (arrow), relative to

1167     untreated WT neutrophils (**a**). (**d**) NOD-SCID mice injected with IFNλ-exposed LCN-2$^{-/-}$

1168     neutrophils showed relatively lower numbers of neutrophils in the eye (arrow) (**i** and **iv**), with

1169     respect to IFNλ-treated WT neutrophils (**c**), especially in the (**ii**) retina (arrow). There was no

1170     visible neutrophil infiltration into (**iii**) Schlemm's canal. n=1. Scale bar, 300 μm

1171

1172

1173

1174

1175

1176

1177

1178

1179

1180

1181
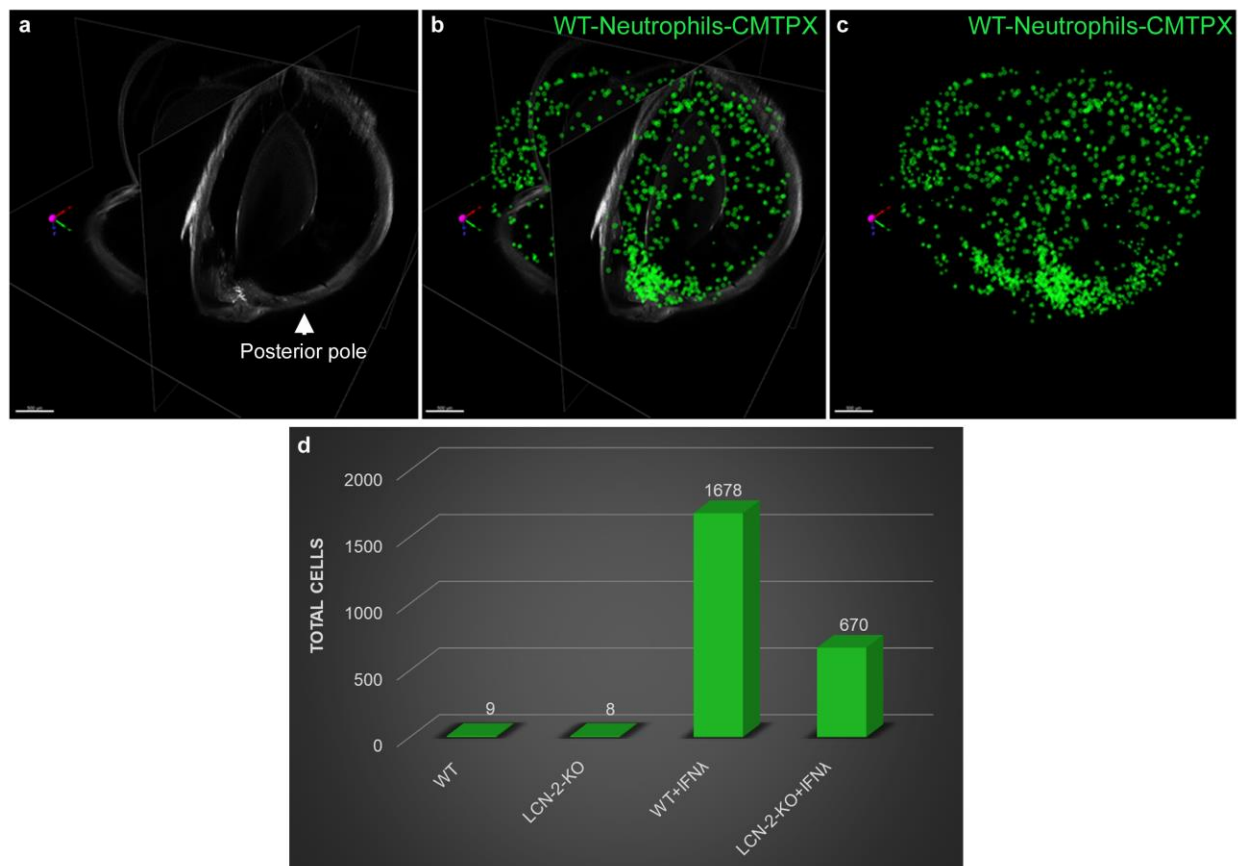
1182

**Fig. 5. LCN-2 is responsible for neutrophil sequestration into the eye**. (**a**) Orthogonal

projections from all three dimensions of a whole eye from a mouse injected with WT neutrophils

+ IFNλ. Cells within the retina and Schlemm's canal were extracted as spot counts in Imaris

software. Cells are depicted as green spheres (**b**) with and (**c**) without the orthogonal projection.

(**d**) Counts extracted from all groups demonstrated an increase in neutrophil number (cell count)

in the NOD-SCID mice injected (intravenous) with IFNλ-treated WT

neutrophils compared to untreated controls, whereas loss of LCN-2 in neutrophils (LCN-2$^{-/-}$)

showed reduced infiltration even after IFNλ exposure. n=1. Scale bar, 500 μm.

1191

1192

1193

**a**

**(i) Vehicle control**
GCL, IPL, INL, OPL, ONL, OLM, IS+OS, RPE

**(ii) WT neutrophils**
GCL, IPL, INL, OPL, ONL, IS+OS, RPE

**(iii) WT neutrophils + IFNλ**
GCL, IPL, INL

**(iv) WT neutrophils + IFNλ cond. media**
GCL, IPL

**(v) Recombinant LCN-2**
GCL, IPL

**(vi) LCN-2⁻/⁻ neutrophils**
GCL, IPL, INL, OPL, ONL, OLM, IS+OS, RPE

**(vii) LCN-2⁻/⁻ neutrophils + IFNλ**
GCL, IPL, INL, OPL, ONL, OLM, IS+OS, RPE

**(viii) LCN-2⁻/⁻ neutrophils + IFNλ cond. media**
GCL, IPL, INL, OPL, ONL, OLM, IS+OS, RPE

**(ix)** IS/OS + RPE thickness (μm) vs Distance from ONH (mm)

- Vehicle control
- WT neutrophils
- WT neutrophils + IFNλ
- WT neutrophils + IFNλ cond. media
- Recombinant LCN-2
- LCN-2⁻/⁻ neutrophils
- LCN-2⁻/⁻ neutrophils + IFNλ
- LCN-2⁻/⁻ neutrophils + IFNλ cond. media

**b**

**(i) Vehicle control** — GCL, IPL, INL, ONL, IS+OS, RPE, Choroid

**(ii) WT neutrophils** — GCL, IPL, INL, ONL, IS+OS, RPE, Choroid

**(iii) WT neutrophils + IFNλ** — GCL, IPL, INL, ONL, IS+OS, RPE, Choroid

**(iv) WT neutrophils + IFNλ cond. media** — GCL, IPL, INL

**(v) Recomb. LCN-2** — GCL, IPL, INL, ONL

**(vi) LCN-2⁻/⁻ neutrophils** — GCL, IPL, INL, ONL, IS+OS, RPE, Choroid

**(vii) LCN-2⁻/⁻ neutrophils + IFNλ** — GCL, IPL, INL, ONL, IS+OS, RPE, Choroid

**(viii) LCN-2⁻/⁻ neutrophils + IFNλ cond. media** — GCL, IPL, INL, ONL, IS+OS, RPE, Choroid

**(ix)** IS/OS + RPE thickness (μm) vs Distance from ONH (mm)

- Vehicle control
- WT neutrophils
- WT neutrophils + IFNλ
- WT neutrophils + IFNλ cond. media
- Recombinant LCN-2
- LCN-2⁻/⁻ neutrophils
- LCN-2⁻/⁻ neutrophils + IFNλ
- LCN-2⁻/⁻ neutrophils + IFNλ cond. media

**Fig. 6. LCN-2 laden neutrophils promote AMD-like pathology.** (**a**) Representative spectral-OCT images of retinas from NOD-SCID mice injected sub-retinally with (**i**) vehicle (HBSS) or

57

1197 (**ii**) WT neutrophils revealed normal retinal structure. In contrast, mice injected with; WT

1198 neutrophils pre-treated with either (**iii**) recombinant IFNλ (200 U/mL), (**iv**) conditioned media

1199 from IFNλ overexpressing mouse RPE cells (1:1 diluted) or (**v**) recombinant LCN-2 (10 pg/mL),

1200 show apparent changes in the ONL and INL layers (asterisks), concomitant with severe loss of

1201 RPE and IS+OS layer (yellow arrow heads). These alterations were not observed in mice

1202 injected with; (**vi**) untreated neutrophils from LCN-2$^{-/-}$ mice or (**vii-viii**) IFNλ-exposed LCN-2$^{-/-}$

1203 neutrophils. (**ix**) Representative spider plot showing the thickness of the IS/OS+RPE layers using

1204 the OCT images among the experimental groups. n=10. $^{*}P<0.05$ (one-way ANOVA and Tukey's

1205 post-hoc test) (**b**) Hematoxylin-eosin staining showed no noticeable alterations in; (**i**) vehicle

1206 treated or mice injected with untreated (**ii**) WT or (**vi-viii**) LCN-2-/- neutrophils (+/-) IFNλ. But,

1207 significant alterations were observed in the INL or ONL (blue asterisks) and RPE/IS+OS (blue

1208 arrow heads), in NOD-SCID mice sub-retinally injected with; (**iii-iv**) IFNλ-exposed WT

1209 neutrophils or (**v**) recombinant LCN-2. (**ix**) Representative spider plot from all of the

1210 experimental groups showing the thickness of the IS/OS + RPE layers using the H&E images.

1211 n=5. $^{*}P<0.05$ (one-way ANOVA and Tukey's post-hoc test), Scale Bar, 20 μm.

1212

1213

1214

1215

1216

1217

1218

1219
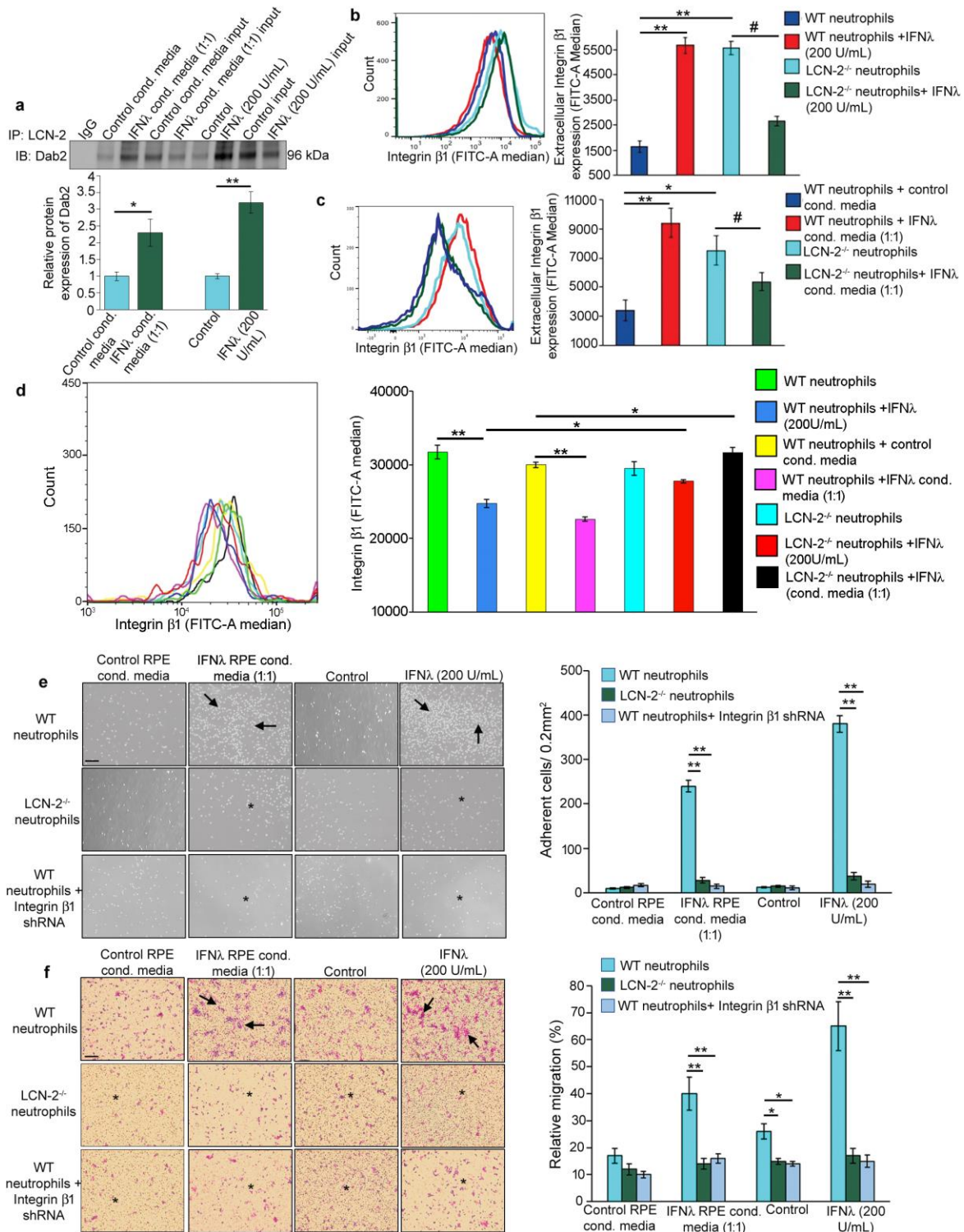
1220

**Fig. 7. LCN-2 regulates neutrophil adhesion and transmigration by modulating the**

**Dab2/integrin β1 axis. (a)** Pull down assay from neutrophils exposed to conditioned media from

RPE cells overexpressing IFNλ (1:1, for 6 h) or to recombinant IFNλ (200 U/mL, for 2 h)

1224    showed increased association between LCN-2 and Dab2 upon IFNλ treatment, relative to

1225    control. n=3. *$P< 0.05$ and **$P< 0.01$ (one-way ANOVA and Tukey's post-hoc test). (**b, c and**

1226    **d**) Flow cytometry assay showed increased extracellular and decreased intracellular expression

1227    of integrin β1 (FITC-A Median) respectively, in WT neutrophils treated with either recombinant

1228    IFNλ (200 U/mL, 2 h) or conditioned media from RPE cells overexpressing IFNλ (1:1 diluted, 6

1229    h), compared to controls. Absence of LCN-2 in neutrophils (LCN-2$^{-/-}$) led to a reversal in the

1230    expression of both extracellular and intracellular levels on integrin β1, even after IFNλ

1231    treatment, relative to WT neutrophils. n=3. *$P<0.05$, **$P< 0.01$ and $^{#}P<0.05$ (one-way ANOVA

1232    and Tukey's post-hoc test). (**e, f**) WT and LCN-2$^{-/-}$ neutrophils exposed to IFNλ (recombinant

1233    200 U/mL for 2 h or 1:1 diluted conditioned media from RPE cells overexpressing IFNλ for 6 h),

1234    showed rapid adhesion to fibrinogen (20 mg/mL) coated plates (top panel, arrows: graph denotes

1235    adherent cells, counted in 0.2 mm$^{2}$) and transmigration across fibrinogen (150 mg/mL) coated

1236    plates (bottom panel, arrows: graph denotes relative migration (%) of cells, representative of cell

1237    count at the bottom of the insert using a computer assisted cell counter system). Integrin β1

1238    shRNA transfected and LCN-2$^{-/-}$ neutrophils do not show changes in adhesion and

1239    transmigration even after IFNλ exposure (asterisk) n=4. *$P< 0.05$ and **$P< 0.01$ (one-way

1240    ANOVA and post-hoc test). Scale bar, 50 μm.

1241

1242

1243

1244

1245

1246
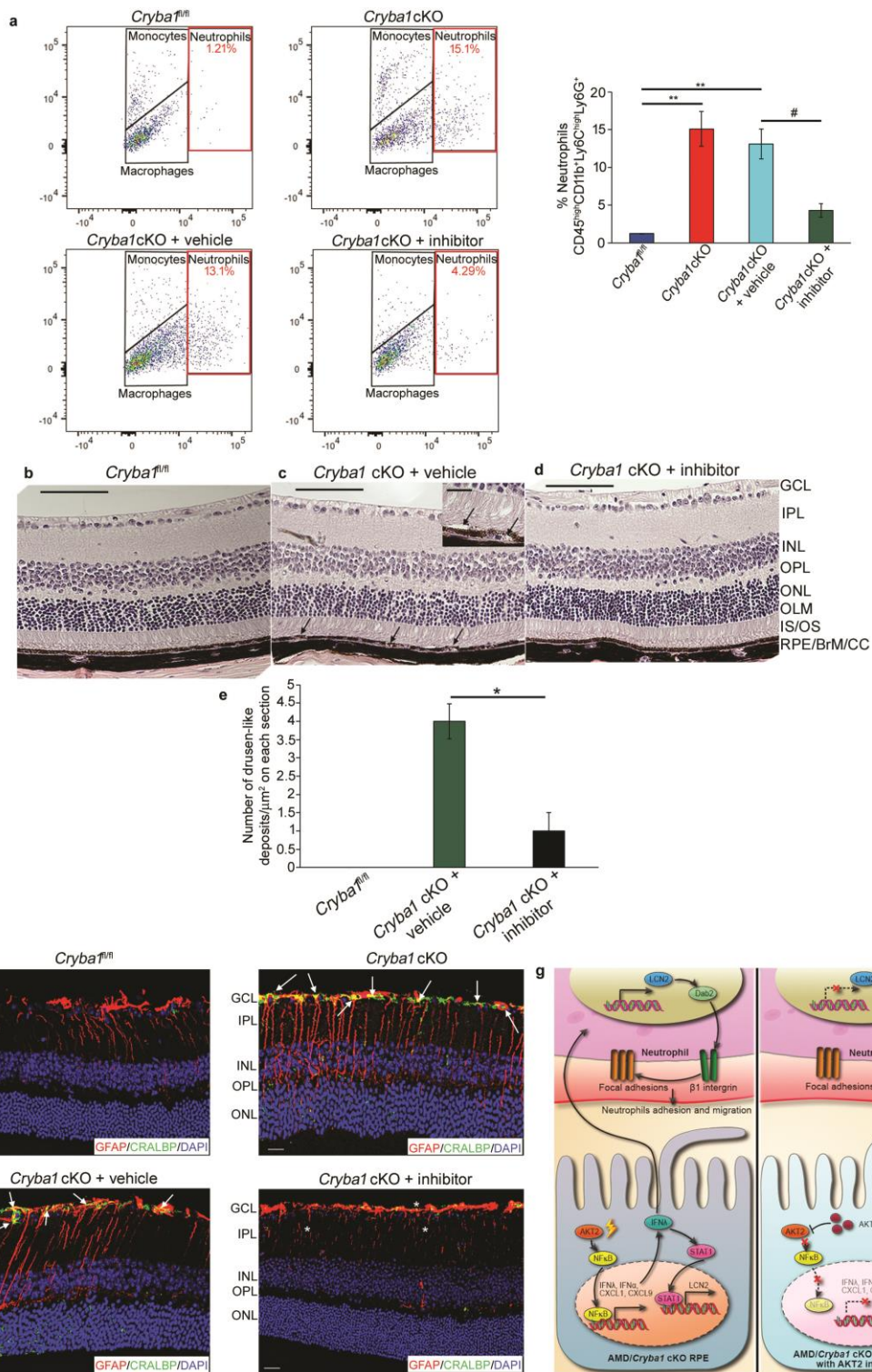
1247

**Fig. 8. Inhibiting AKT2 phosphorylation blocks neutrophil infiltration into the retina and rescues early RPE changes in *Cryba1* cKO mice**. (**a**) Flow cytometry dot plots denoting monocytes, macrophages and neutrophils from mouse retina (as explained in Fig. 1a). The

1251  neutrophil population (%CD45$^{high}$CD11b$^+$Ly6C$^{high}$Ly6G$^+$ cells, red gated) significantly increased

1252  in the 12 month *Cryba1* cKO mouse retina +/- intravitreal vehicle treatment, compared to age-

1253  matched *Cryba1*$^{fl/fl}$ (control).  Intravitreal treatment with the AKT2 inhibitor (CCT128930)

1254  significantly reduced neutrophils in cKO retina.  Graphs denote %

1255  CD45$^{high}$CD11b$^+$Ly6C$^{high}$Ly6G$^+$ cells. n=4. **$P< 0.01$ and $^\#P< 0.05$ (one-way ANOVA and

1256  post-hoc test). (**b-d**) Representative histological sections (H&E) of retina from 1 year old

1257  *Cryba1*$^{fl/fl}$ mouse, showing normal structure (**b**). Age-matched *Cryba1* cKO mouse (**c**)

1258  intravitreally injected with vehicle (2.5% DMSO in PBS) shows RPE and photoreceptor lesions

1259  with pigmentation changes (arrows). Inset in **c**, shows higher magnification of RPE lesions

1260  indicating possible debris accumulation between Bruch's membrane and RPE and separation of

1261  photoreceptors from RPE (arrows). In contrast, inhibitor (CCT128930, inhibits AKT2 activation)

1262  treated *Cryba1* cKO mice (**d**), exhibited normal structure after 4 weeks. (**e**) Bar graph showing

1263  decrease in number of sub-retinal drusen-like deposits after AKT2 inhibitor treatment compared

1264  to vehicle-treated cKO mice. n=4. Scale bars, 100 μm and 50 μm (inset). *$P< 0.05$ (one-way

1265  ANOVA and post-hoc test). (**f**) Retina sections from 12 month old *Cryba1*$^{fl/fl}$ or *Cryba1* cKO

1266  mice stained with glial fibrillary acidic protein (GFAP, red) and cellular retinaldehyde-binding

1267  protein (CRALBP, green).  Sections from cKO mice +/- intravitreal vehicle showed extensive

1268  staining of the Muller glial processes (cells staining for both CRALBP and GFAP, yellow

1269  indicating activation, arrows). This was significantly reduced after inhibitor treatment (asterisk).

1270  n=4. Scale Bar, 50 μm. (**g**) Schematic depicting neutrophils homing into the retina and releasing

1271  LCN-2, generating pro-inflammatory conditions that contribute to elements of early AMD

1272  pathobiology. Our data suggest that IFNλ triggers transmigration of neutrophils into the retina

1273  through activation of the LCN-2/Dab2/integrin β1 signaling axis (Left panel). Inhibiting AKT2-

1274 dependent signaling can neutralize inflammatory signals and block neutrophil infiltration (Right

1275 Panel). Thus, AKT2 inhibitors should be assessed as potential therapy at the earliest stages of

1276 AMD.

1277

1278

1279

1280

1281

1282

1283

1284

1285

1286

1287

1288

1289

1290

1291

1292

1293

1294

1295

1296

**Supplementary Materials**
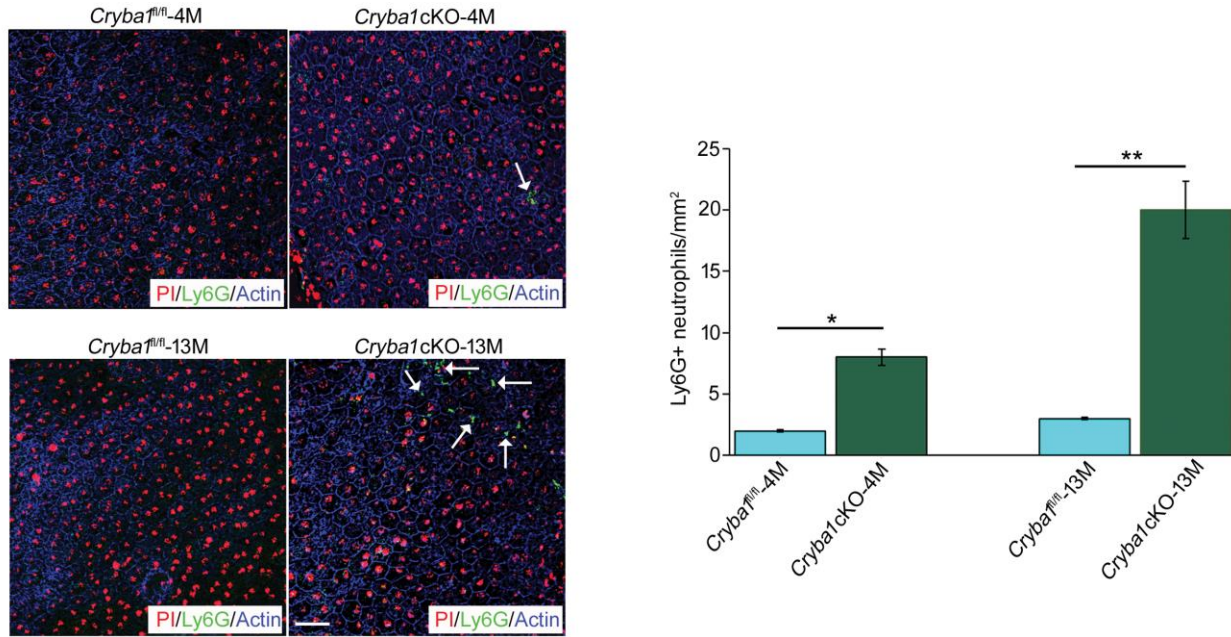


1298

**Supplementary Fig. 1. Sub-retinal accumulation of neutrophils in *Cryba1* cKO mice.**

Immunofluorescence studies followed by quantification of Ly6G$^+$ cells (Green, Neutrophil

marker) on RPE flatmounts, counterstained with propidium iodide (PI, Red, which stains nuclei)

and actin (Blue) showed significant increase in Ly6G$^+$ neutrophils in *Cryba1* cKO mice as a

function of age, relative to floxed controls (*Cryba1*$^{fl/fl}$). n=4. *$P < 0.05$, **$P < 0.01$ (One-way

ANOVA and Tukey's post-hoc test). Scale bar, 50 μm.

1305

1306

1307

1308

1309

1310

1311
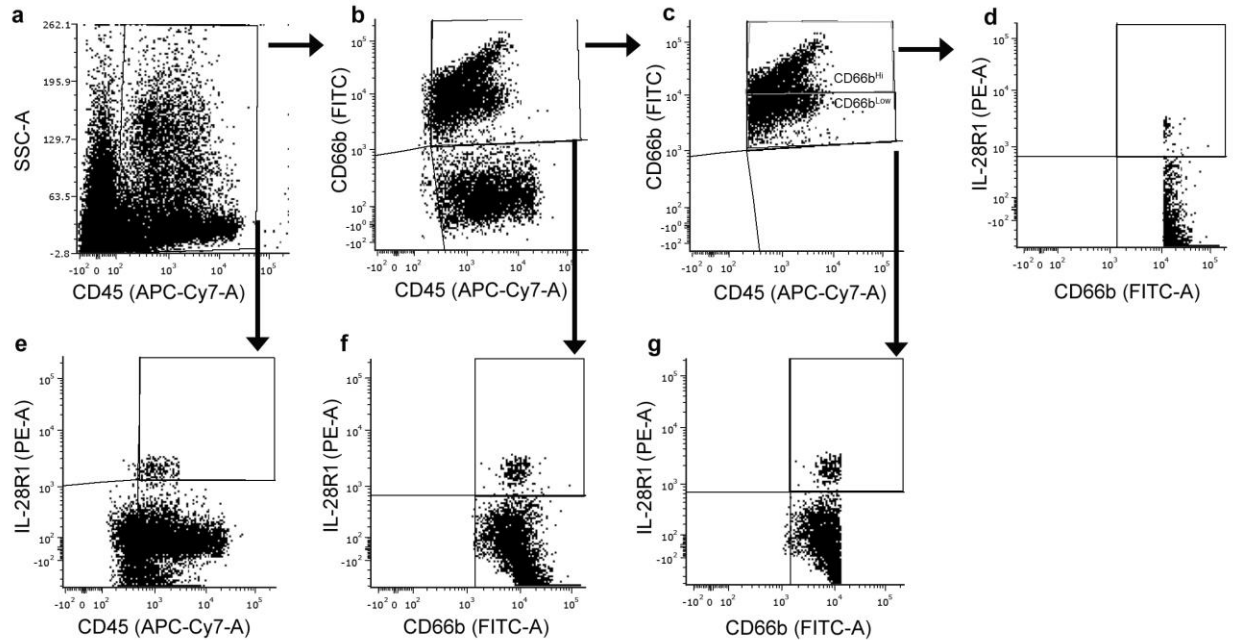
1312

**Supplementary Fig. 2. Gating strategies for immune cell populations from human samples.**

Representative images showing gating strategies to evaluate the immune cell populations in the

peripheral blood samples from control and AMD subjects. The cells from respective samples

were stained for different cell surface markers and serial gating strategies (marked with black

arrows) were performed among leukocytes (CD45$^+$ cells). (**a**) CD45 (APC-Cy7-A, leukocytes)

vs Side Scatter (SSC-A), representing the leukocytes population in the different samples. The

CD45$^+$ cells were further used to evaluate other cell populations in the samples. (**b**)

CD45$^+$CD66b$^+$ (neutrophils) cells were gated from the total CD45$^+$ leukocytes from 'a'. (**c**)

Representative gating denoting CD45$^+$CD66b$^{high}$ (activated neutrophils) and CD45$^+$CD66b$^{low}$

(naive neutrophils) population of cells among the CD66b$^+$CD45$^+$ neutrophils from 'b'. (**d**)

CD66b$^{high}$IL28R1$^+$ (activated neutrophils expressing IFNλ receptor) cells were gated from the

CD66b$^{high}$ population from 'c'. (**e**) Leukocytes expressing IFNλ receptor (CD45$^+$IL28R1$^+$) were

gated from the total CD45$^+$ cells (in 'a') from each sample. (**f**) Neutrophils (CD66b$^+$ cells)

expressing IFNλ receptor (CD66b$^+$IL28R1$^+$) were gated from the total CD45$^+$CD66b$^+$ cells (in

1327    'b') from each sample. (**g**) Naive neutrophils expressing IFNλ receptor (CD66b$^{low}$IL28R1$^{+}$) were

1328    gated from the CD45$^{+}$CD66b$^{low}$ cell population from 'c'.

1329

1330

1331

1332

1333

1334

1335

1336

1337

1338

1339

1340

1341

1342

1343

1344

1345

1346

1347

1348

a



b



c

(i) Control

(ii) AMD

(iii) AMD

(iv) AMD

(v)
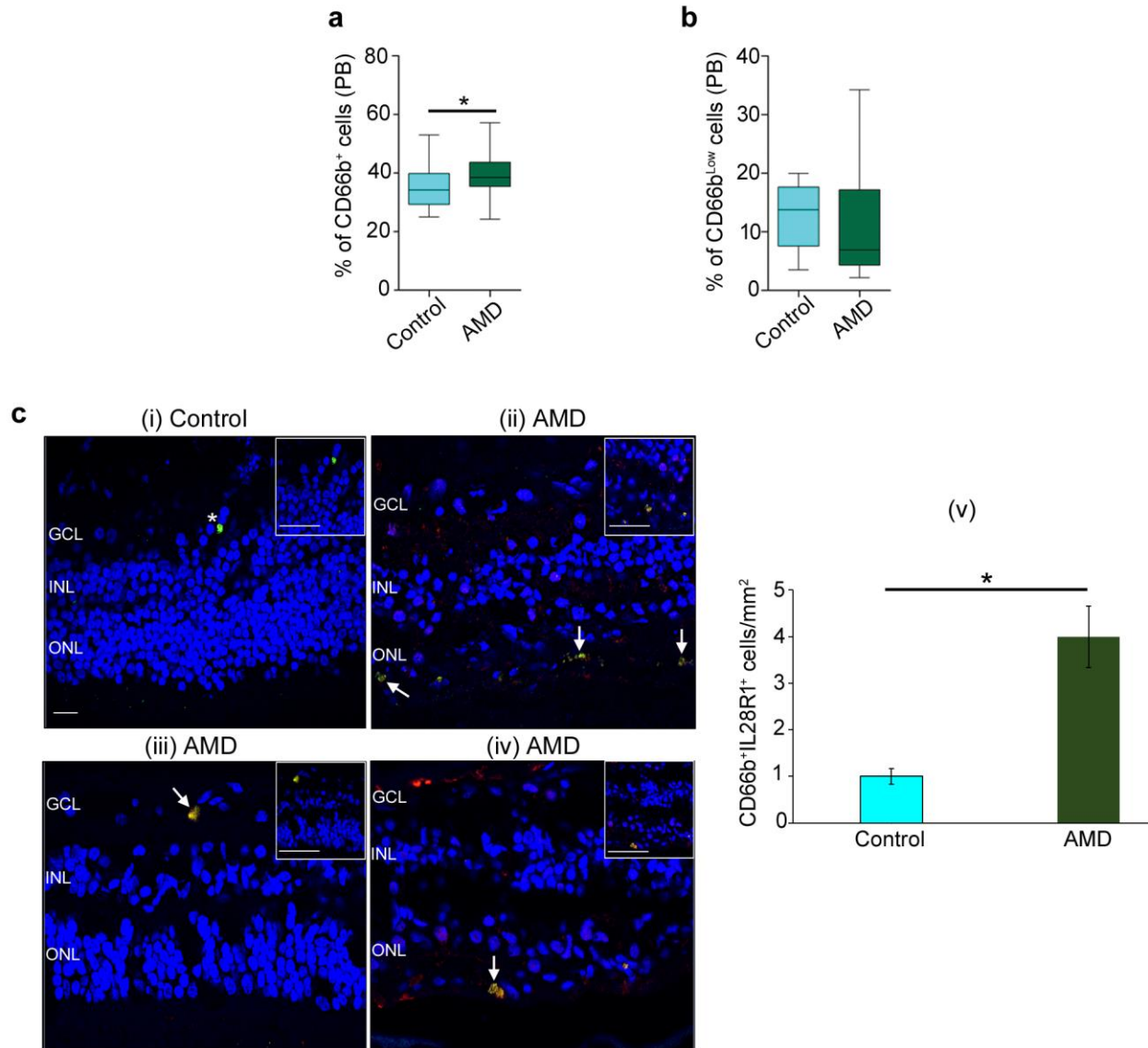
1349

**Supplementary Fig. 3. Immune cell analysis in peripheral blood of human early AMD**

**patients.** Flow cytometry analysis (gated as described in Fig. S2) showing significant change in

(**a**) total CD66b$^+$ cells (neutrophils) in peripheral blood (PB), of AMD patients compared to

controls, with no significant change in the levels of CD66b$^{low}$ cells (naïve neutrophils) (**b**).

Peripheral blood (AMD; n=43 and Controls; n=18). *$P$<0.05. Note: $P$-value for B: 0.06 (Mann-

Whitney test). (**c**) Immunofluorescence study followed by quantification for CD66b$^+$

(neutrophils) IL28R1$^+$ (IFNλ receptor) double positive cells, showed increased prevalence of

1357     CD66b$^+$IL28R1$^+$ cells (arrows, inset showing zoomed image of the region of interest) in retinal

1358     sections from human AMD patients (**ii-v**), compared to control subjects (**i and v**) which showed

1359     a lower number of CD66b+ neutrophils with no expression of IL28R1 in these cells (asterisk).

1360     n=3. *$P < 0.05$ (One-way ANOVA and Tukey's post-hoc test). Scale bar, 50 μm (Inset: 20 μm).

**a**

(i) AMD

DAPI/NE/MPO

(ii) AMD

DAPI/NE/MPO

(iii) Control

DAPI/NE/MPO

**b**

(i) AMD

DAPI/Citrullinated Histone H3/NE

(ii) AMD

DAPI/Citrullinated Histone H3/NE

(iii) Control

DAPI/Citrullinated Histone H3/NE
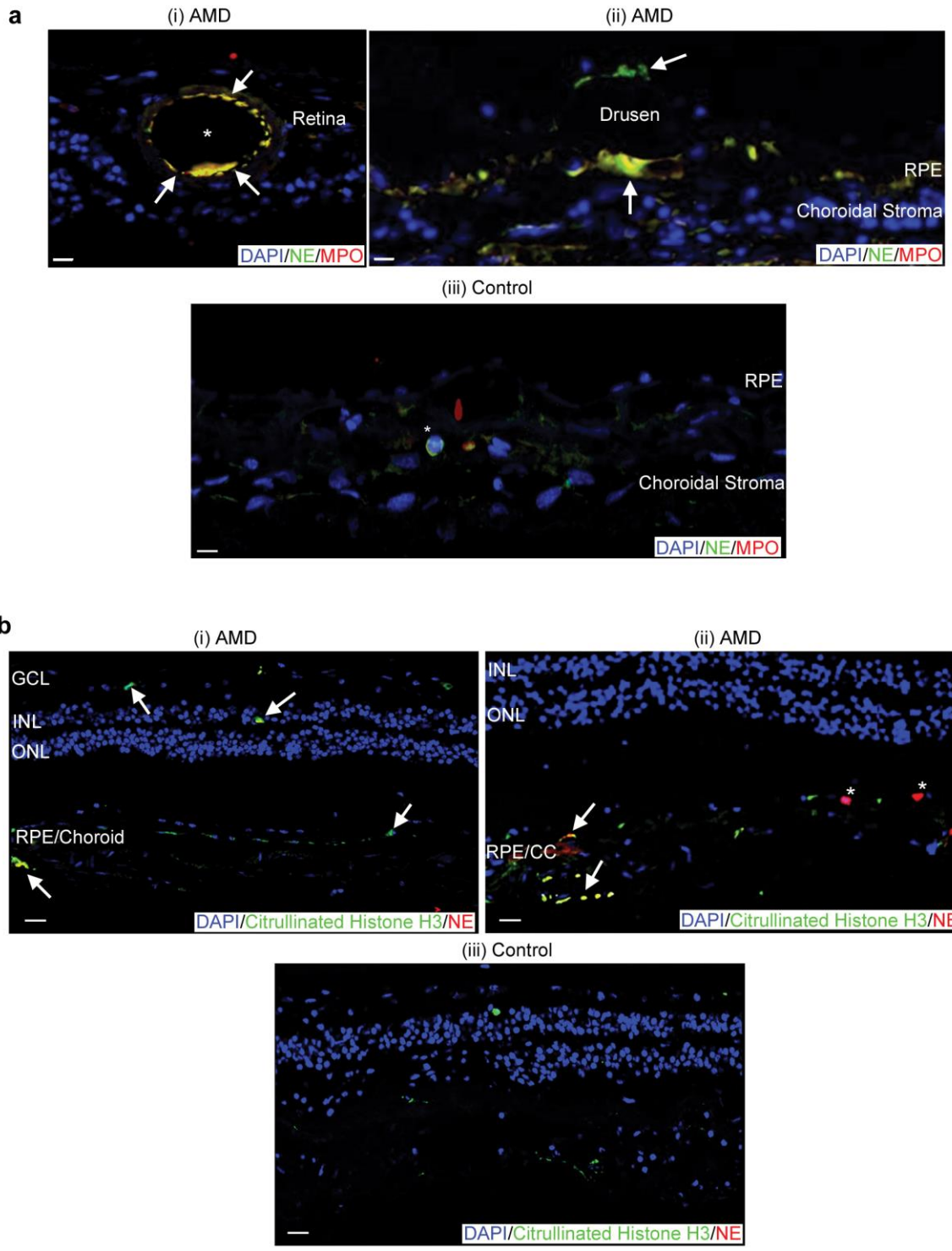
**Supplementary Fig. 4. Increased expression of neutrophil extracellular traps in infiltrating neutrophils in human AMD retina.** (**a**) NE (Neutrophil elastase, Green) and MPO (Myeloperoxidase, Red) immunostaining of the tissue sections from early AMD donors revealed

that MPO/NE positive neutrophils (Yellow, white arrows) (**i**) lined the retinal blood vessel

(asterisk) and (**ii**) the surface of drusen deposits under the retina (white arrows). (**iii**) Control

sections showed fewer neutrophils, which did not stain for MPO (asterisk). n=3. Scale bar, 50

µm. (**b**) Immunofluorescent staining of, (**i, ii**) human AMD sections revealed increased staining

for citrullinated histone H3 (Green) among neutrophil elastase (NE, Red) positive neutrophils in

the retina and choroid (Yellow, white arrows) compared to (**iii**) age-matched controls. n=3. Scale

bar, 50 µm.

|  | 5M | | 10M | | |
|---|---|---|---|---|---|
|  | *Cryba1*fl/fl | *Cryba1* cKO | *Cryba1*fl/fl | *Cryba1* cKO | |
| CXCL1 | | | | | **P<0.01 |
| CXCL9 | | | | | **P<0.01 |
| IFNg | | | | | **P<0.01 |
| IFNa | | | | | **P<0.01 |
| IFNl | | | | | **P<0.01 |
| IFNgr1 | | | | | |
| IFNgr2 | | | | | |
| IFNar1 | | | | | |
| IFNar2 | | | | | |
| IFNlr1 | | | | | |
| IL-6 | | | | | *P<0.05 |
| IL1b | | | | | *P<0.05 |
| IL1a | | | | | *P<0.05 |
| TNFa | | | | | *P<0.05 |
| TGFb1 | | | | | *P<0.05 |
| TGFb2 | | | | | |
| TGFb3 | | | | | |
| TGFa | | | | | *P<0.05 |
| CXCL2 | | | | | *P<0.05 |
| CXCL14 | | | | | *P<0.05 |
| IL-13 | | | | | |
| IL-15 | | | | | |
| IL-21 | | | | | |
| IL-27 | | | | | |
| IL-3 | | | | | |
| IL-33 | | | | | |
| IL-5 | | | | | |
| IL-7 | | | | | |
| CCL1 | | | | | *P<0.05 |
| CCL11 | | | | | |
| CCL16 | | | | | |
| CCL17 | | | | | *P<0.05 |
| CCL2 | | | | | |
| CCL22 | | | | | |
| CCL5 | | | | | |
| CXCL10 | | | | | |
| CXCL12 | | | | | |
| CXCL13 | | | | | *P<0.05 |
| CXCL5 | | | | | |
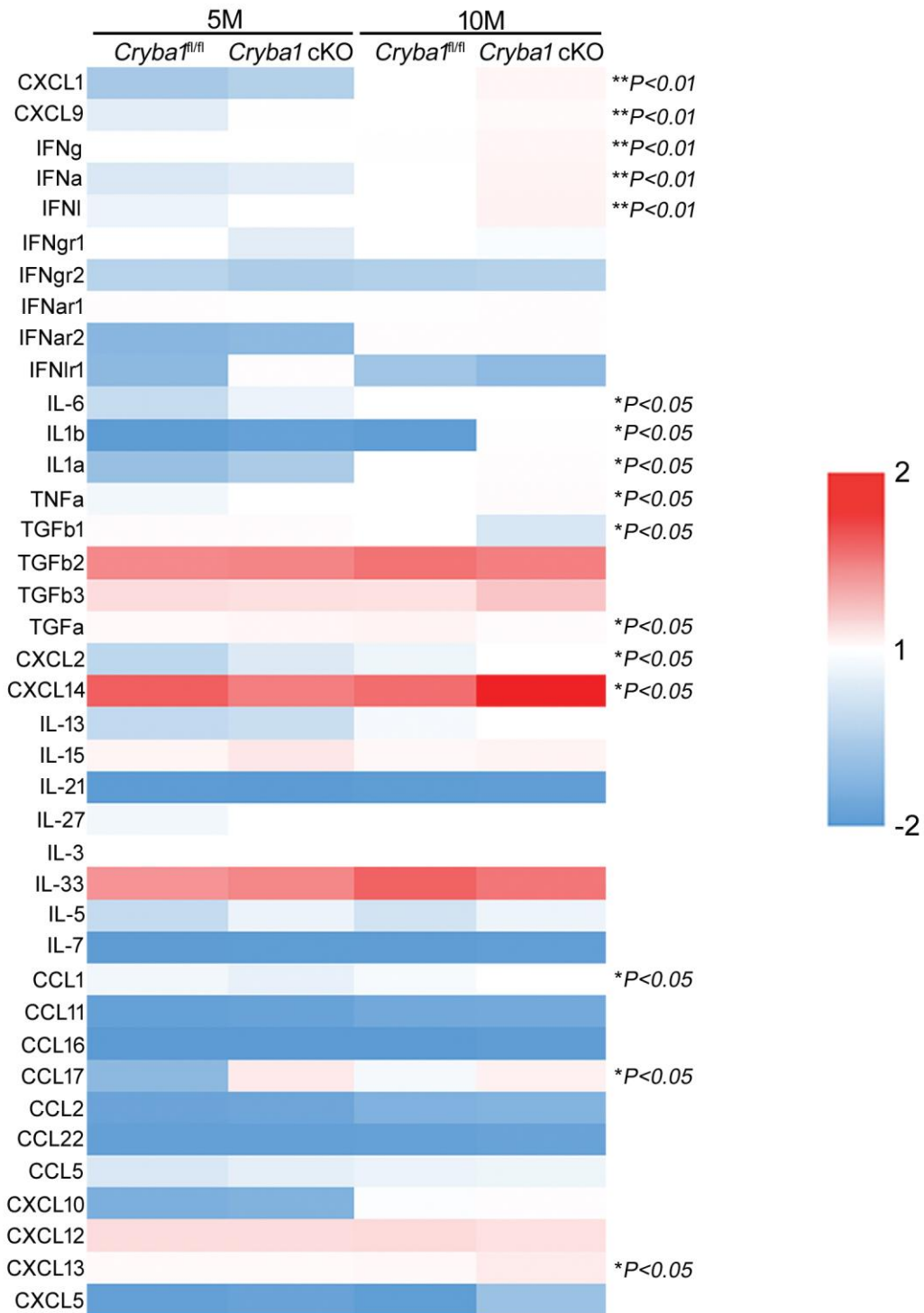
1386

**Supplementary Fig. 5. Increased transcription of neutrophil-regulating molecules in the RPE/Choroid of mice with AMD-like pathology.** Heat map of RNAseq analysis from retina of 5 and 10 month old *Cryba1*fl/fl and *Cryba1* cKO, focusing mainly on the expression of

71

1390    inflammatory genes. Significant increase in RNA levels of neutrophil regulating molecules like

1391    CXCL1, CXCL9 and IFN-family members such as; IFN Type-I (IFNα, IFNβ), Type-II (IFNγ),

1392    and IFN Type-III (IFNλ) in retina extracts from 10 month old *Cryba1* cKO mice compared to

1393    age-matched *Cryba1*fl/fl (control). No such changes were observed in 5 month old mice, nor were

1394    there differences in expression of various IFN receptors. Represents Fragments Per Kilobase of

1395    transcript per Million mapped reads (FPKM) for each gene and are represented as log10 (counts

1396    per million). n=6. *$P < 0.05$ and **$P < 0.01$ with respect to 10 month old *Cryba1*fl/fl group (One-

1397    way ANOVA and Tukey's post-hoc test).

1398

1399

1400

1401

1402

1403

1404

1405

1406

1407

1408

1409

1410

1411

1412
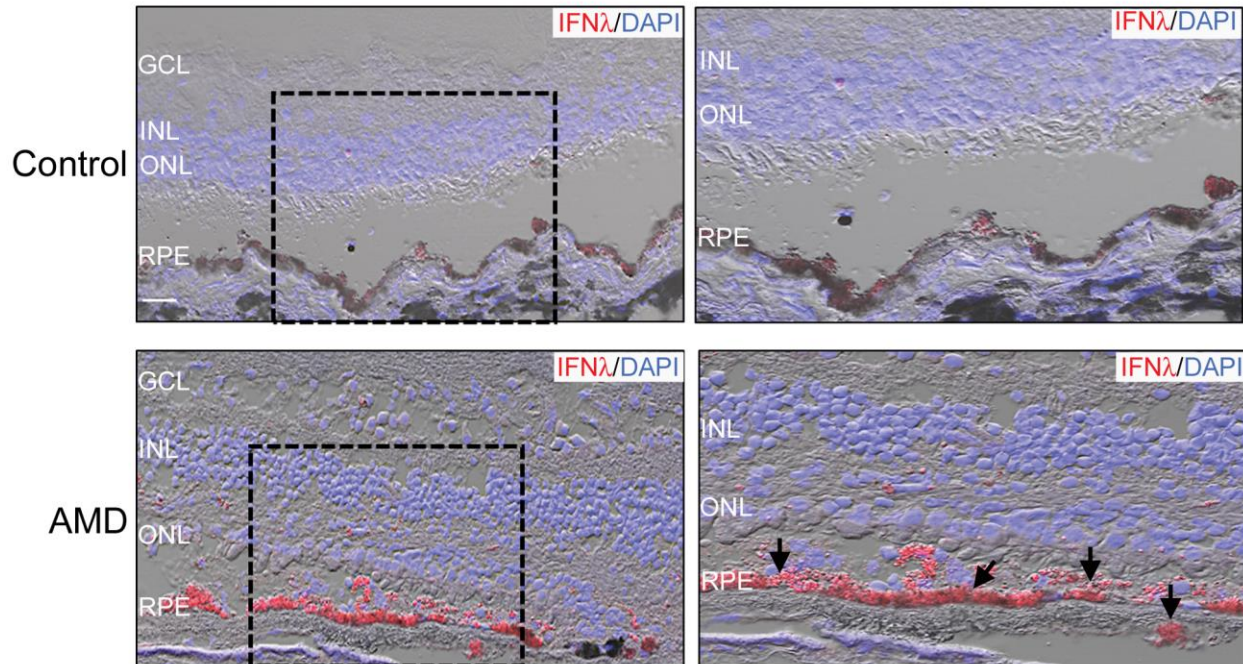
1413

**Supplementary Fig. 6. IFNλ expression in retina of human AMD patient samples.** Increased

IFNλ (Red) immunostaining was apparent in sections from AMD patients relative to age-

matched controls. The RPE cells (indicated by arrows) showed increased staining for the protein

(zoomed image on right panel representative of ROI-marked with dotted line). The control retina

did not show noticeable staining for IFNλ. n=4. Scale Bar, 50 μm.

1419

1420

1421

1422

1423

1424

1425

1426
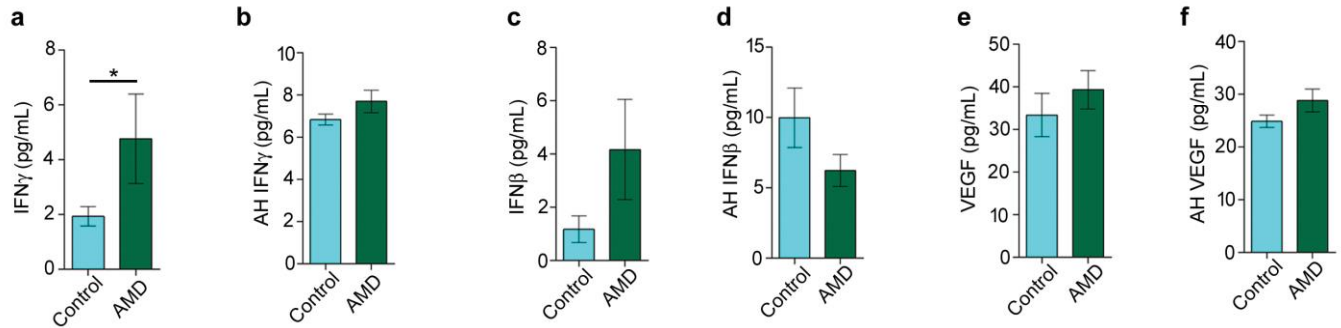
**Supplementary Fig. 7. Expression of neutrophil regulating cytokines in human samples.**

Cytometry bead array revealed significant increase in the level of IFNγ in the peripheral blood (PB) in AMD patient samples (**a**) compared to age-matched controls, but not in aqueous humor (AH) samples (**b**). Levels of IFNβ and VEGF did not show any significant change in the PB (**c, e**) or AH (**d,f**) samples between the two groups. Peripheral blood (AMD; n=43 and Controls; n=18) and aqueous humor (AMD; n=6 and Controls; n=7). *$P < 0.05$ (Mann-Whitney test).

Note: *P*-values for **c-d** are: **c**: 0.09 and **d**: 0.20 (Mann-Whitney test).

**a**



**b**
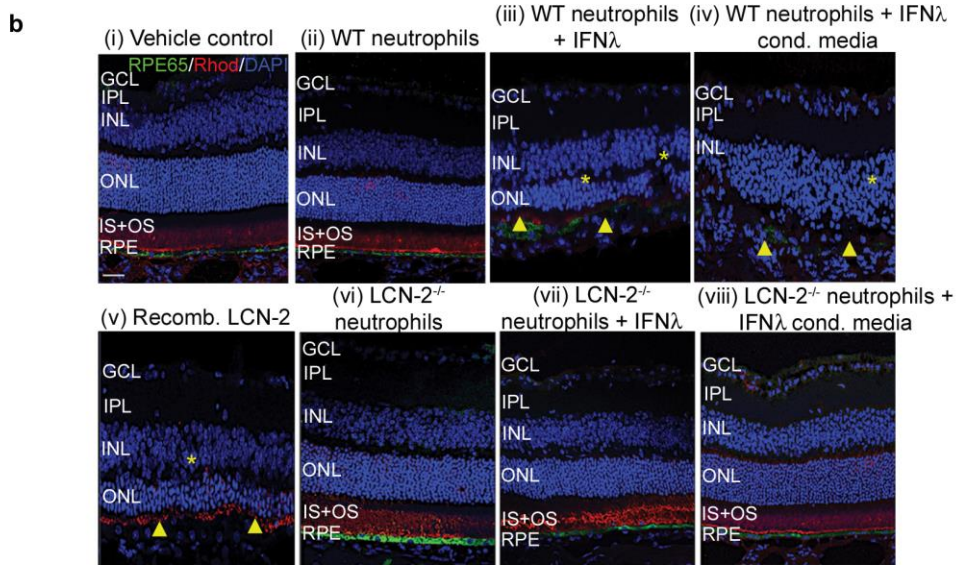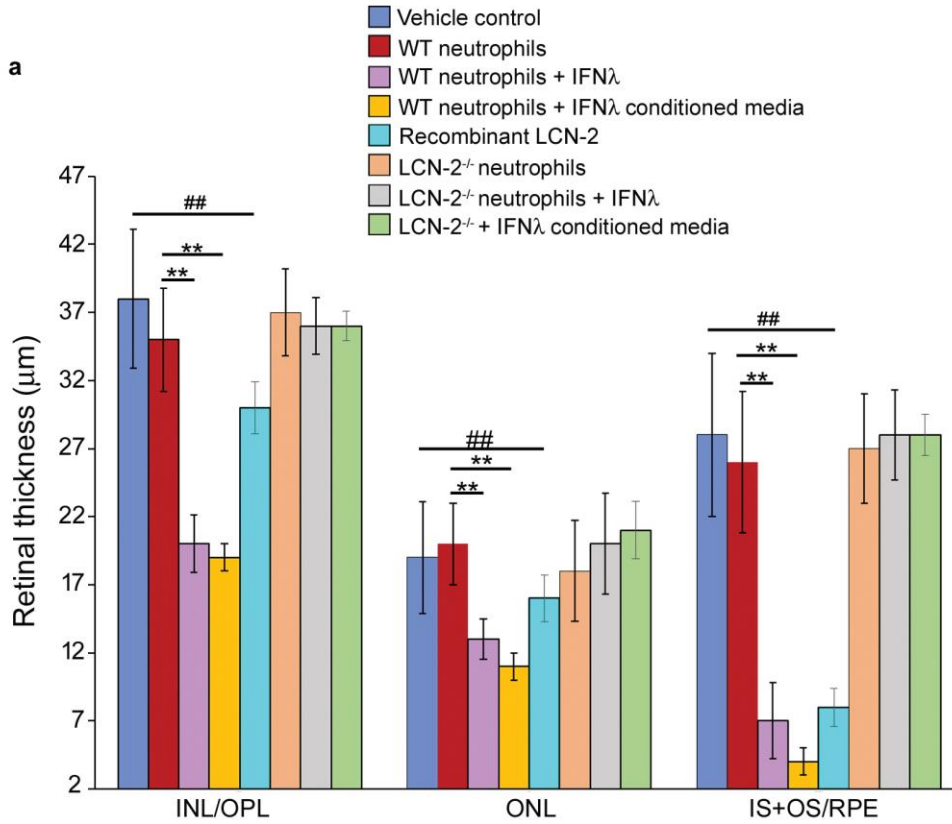


1445

**Supplementary Fig. 8. Alterations in retinal thickness in NOD-SCID mice injected with**

**LCN- 2 or with neutrophils (WT or LCN-2^{-/-}) treated with IFNλ or conditioned medium**

**from RPE cells overexpressing IFNλ. (a)** Sub-retinal injections to NOD-SCID mice (Male, 4-5

75

1449      weeks old) of Recombinant LCN-2 (10 pg/mL) or Wild Type (WT) neutrophils pre-treated with

1450      either conditioned media (1:1 diluted) from IFNλ overexpressing RPE cells (6 h) or 200 U/mL

1451      recombinant IFNλ for 2 h respectively, demonstrated; decreases in INL/OPL, ONL and

1452      IS+OS/RPE thickness compared to vehicle and untreated (control) neutrophil injected groups.

1453      No noticeable changes were observed in mice sub-retinally injected with neutrophils from LCN-

1454      2 KO mice (LCN-2$^{-/-}$ neutrophils), with or without IFNλ exposure. Thickness (μm) analysis was

1455      performed on optical sections (100 sections per retina) from each eye ranging from -2.0 to +2.0

1456      mm with respect to the optic nerve head (ONH). n=10. **$P< 0.01$ with respect to control

1457      neutrophils and $^{##}P<0.01$ with respect to vehicle control (One-way ANOVA and Tukey's post-

1458      hoc test). (**b**) Immunofluorescence assay on retinas from NOD-SCID mice injected sub-retinally

1459      with; (**i**) vehicle or (**iii-iv**) IFNλ-exposed WT neutrophils or (**v**) recombinant LCN-2 revealed

1460      significant loss of IS+OS/RPE layers (yellow arrow heads), evident from decrease in rhodopsin

1461      (Red, a marker for rod photoreceptors) and RPE65 (Green, a marker for RPE cells) staining,

1462      along with noticeable alterations in the INL/ONL layers (yellow asterisks). Mice injected with

1463      (**ii**) WT or (**vi-viii**) LCN-2$^{-/-}$ neutrophils (+/-) IFNλ did not show any change relative to

1464      controls. n=5. Scale Bar, 50 μm.

1465

1466
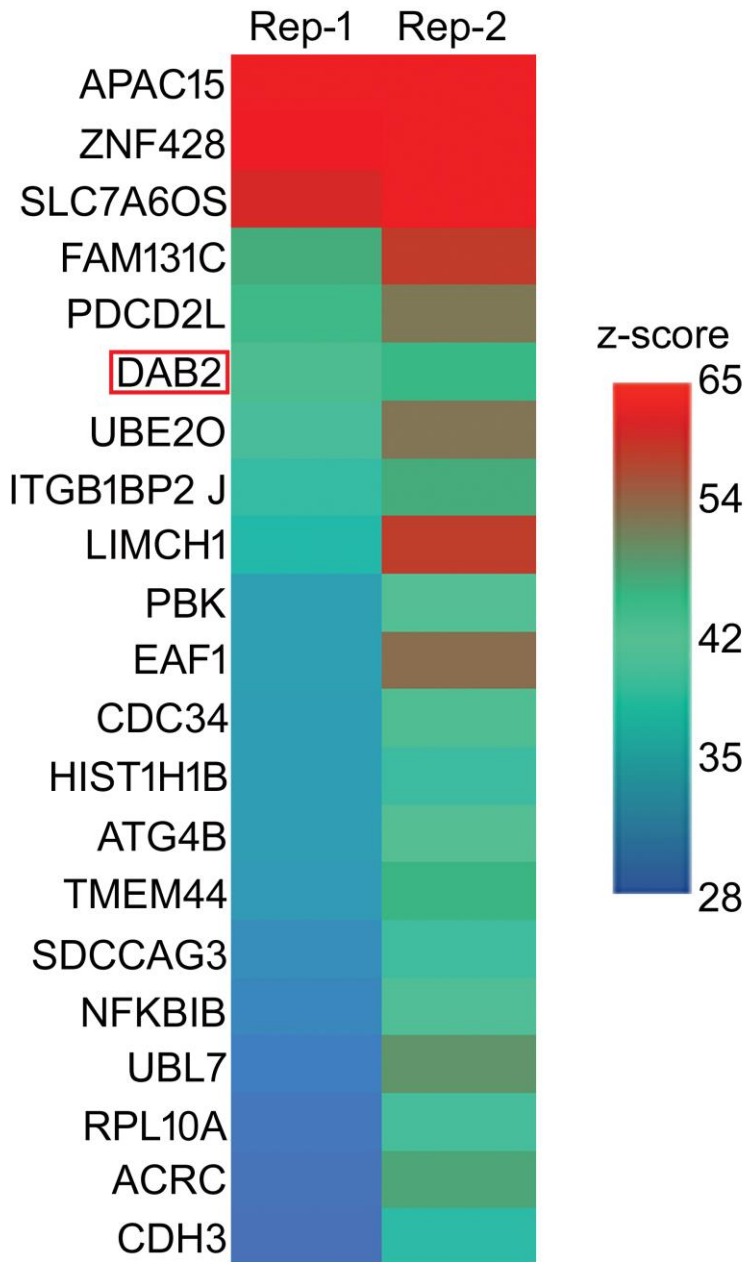
**Supplementary Fig. 9. DAB2 interacts with LCN-2**. Human proteome array showing binding

partners of LCN-2 including DAB2 (red box) probed on HuProtTM arrays at 1 µg/ml.

Represented as z-score (hit for each probe), with a cut-off of 6 and values ranging from 28 to 65.

n=3.
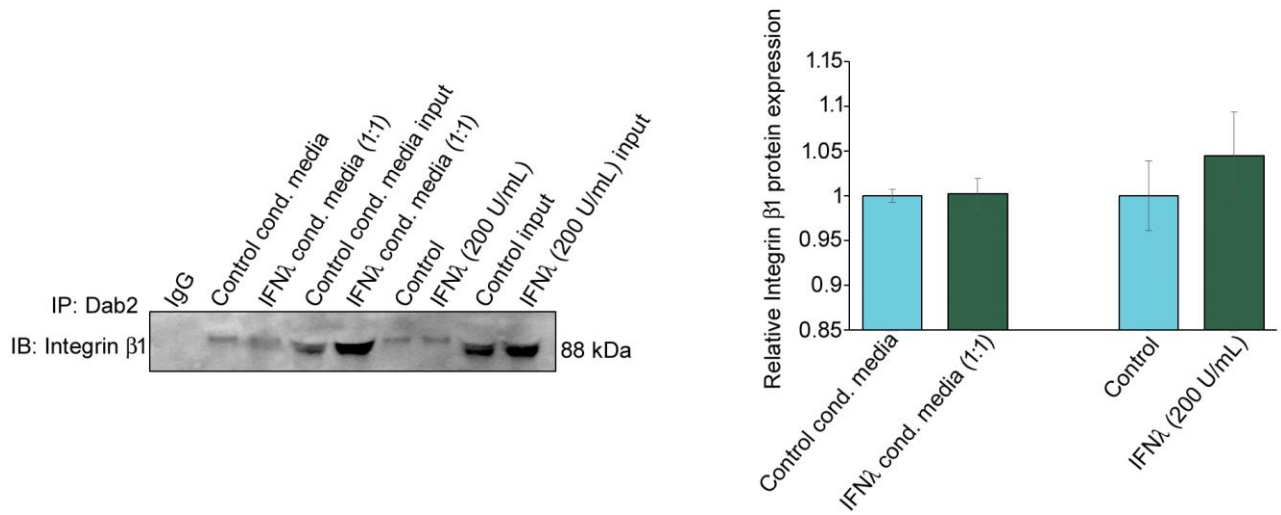
1473

**Supplementary Fig. 10. Dab2 binds to integrin β1**. Pull down assay from immunoprecipitated

Dab2 was used to determine the expression of integrin β1 by western analysis from wild type

neutrophils treated with either recombinant IFNλ (200 U/mL) or IFNλ conditioned media (1:1).

This revealed that Dab2 binds to integrin β1 and there is no noticeable change in the binding

pattern between the two proteins upon IFNλ exposure. n=3.

1479

1480

1481

1482

1483

1484

1485

1486

1487

**a**



**b**
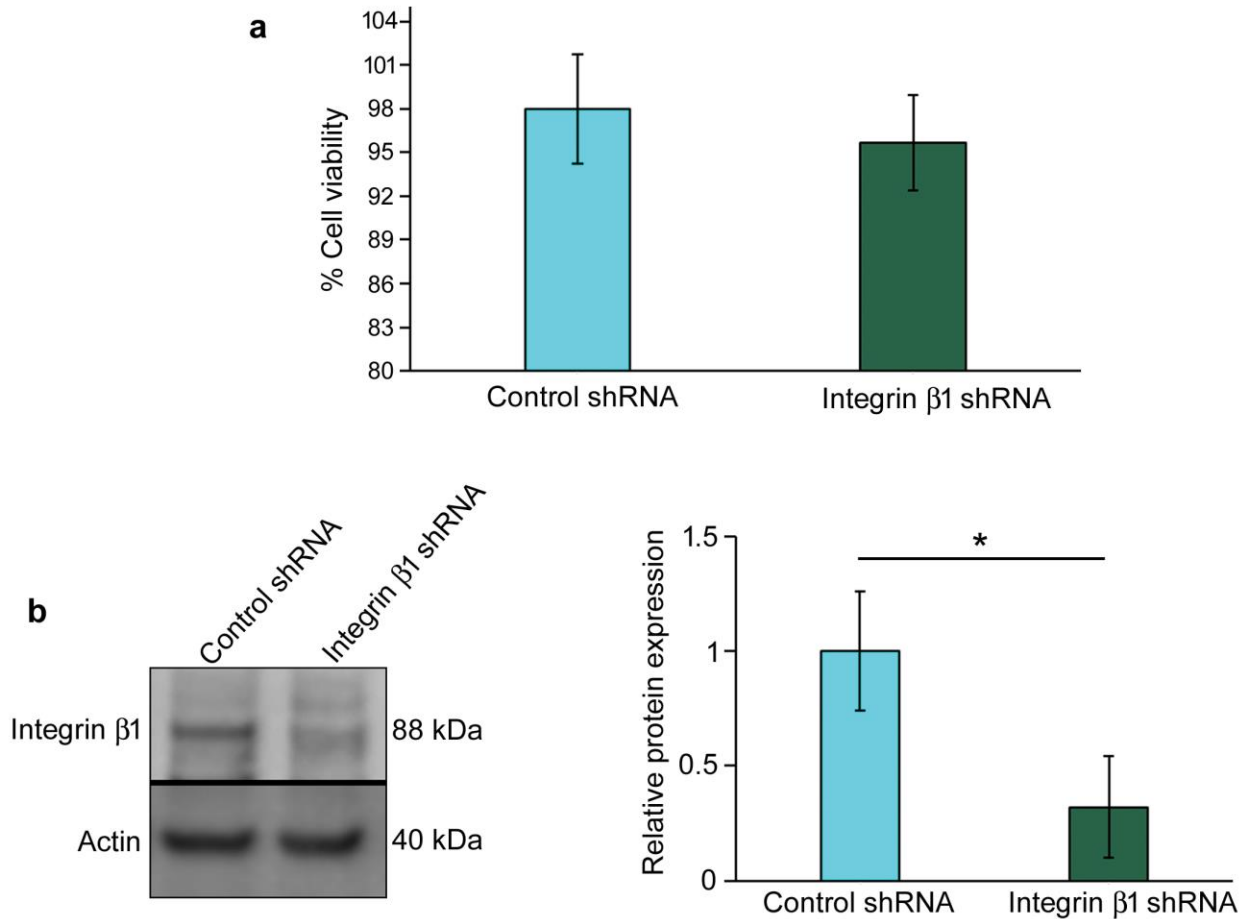
1488

**Supplementary Fig. 11. Inhibition of integrin β1 expression in neutrophils**. Wild type

neutrophils in culture were transfected with integrin β1 shRNA viral particles (see methods). (**a**)

MTT (3-(4,5-Dimethylthiazol-2-Yl)-2,5-Diphenyltetrazolium Bromide) cell viability assay

revealed no significant change in % cell viability between control shRNA and integrin β1

shRNA transfected neutrophils. n=6. (**b**) Decreased expression of integrin β1 as evident from

immunoblot and densitometry among integrin β1 shRNA-transfected neutrophils, relative to

control shRNA transfected cells. n=6. *$P < 0.05$ (one-way ANOVA and Tukey's post-hoc test).

1496

1497
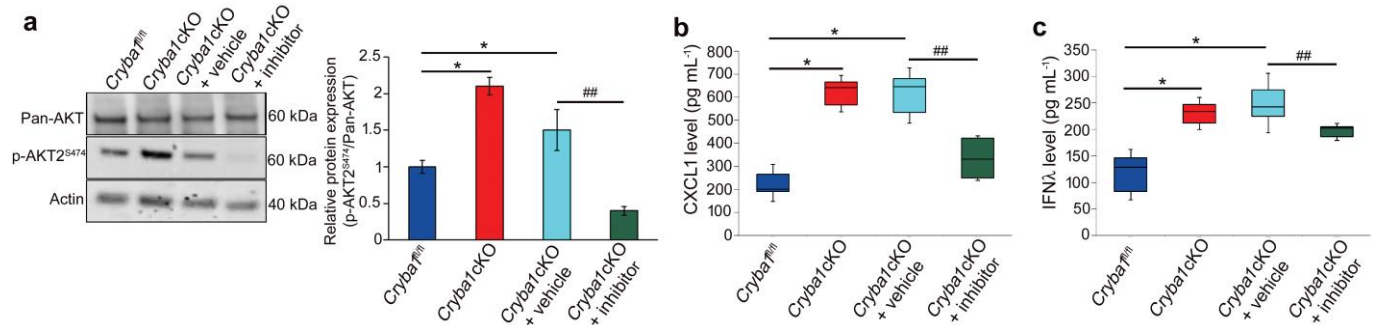
**Supplementary Fig. 12. An AKT2 inhibitor (CCT128930) reduces inflammation in aged**

*Cryba1* **cKO mouse retina.** (**a**) Immunoblot and summary of densitometry showing a significant

increase in the phosphorylation of AKT2 (p-AKT2$^{S474}$) in retinas from 1 year old *Cryba1* cKO

mice. The levels of pAKT2$^{S474}$ in the *Cryba1* cKO RPE decreased significantly following

treatment with inhibitor (CCT128930, at a dose of 500 μM). Vehicle alone (2.5% DMSO in

PBS) had little effect. Additionally, levels of total AKT did not change in the samples. n=3. *$P<$

0.05 with respect to floxed control and $^{\#\#}P<$ 0.01 with respect to vehicle treated *Cryba1* cKO. (**b-**

**c**) ELISA assays show reduced levels (pg/mL) of CXCL1 and IFNλ respectively, in the RPE-

choroid of AKT2 inhibitor-treated *Cryba1* cKO mice, as compared to age-matched vehicle and

untreated *Cryba1* cKO animals. n=3. *$P<$ 0.05 with respect to floxed control and $^{\#\#}P<$ 0.01 with

respect to vehicle treated *Cryba1* cKO.

**Supplementary Table 1: Cohort characteristics of control subjects and AMD patients**

**a**: Cohort details of subjects included for immunophenotyping and soluble factors quantification in peripheral blood and plasma, respectively

|  | Control (n=18) | AMD (n=43) | *P*-value |
|---|---|---|---|
| Age (Mean±SEM; Range) Years | 61.3±14.4; 43-77 | 68.1±10.4;51-88 | 0.016 |
| Gender (M/F) | 10/8 | 23/20 | NA |
| Log Mar (BCVA) RE | 0.08±0.02; 0-0.30 | 0.32±0.05;0-1.61 | 0.010 |
| Log Mar (BCVA) LE | 0.14±0.03; 0-0.78 | 0.20±0.03;0-0.78 | 0.276 |

**b**: Cohort details of subjects included for soluble factors quantification in aqueous humor

|  | Control (n=7) | AMD (n=6) | *P*-value |
|---|---|---|---|
| Age (Mean±SEM; Range) Years | 60.4±3.2;53-76 | 63±3.5;55-76 | 0.462 |
| Gender (M/F) | 3/4 | 3/3 | NA |
| Log Mar (BCVA) | 0.53±0.3;0.1-2.1 | 0.23±0.06;0.03-0.5 | 0.463 |

**Supplementary Table 1. Demographic data for human samples**. Human sample information for immunophenotyping and determination of soluble factors from, (**a**) peripheral blood. (**b**) Information of human aqueous humor samples for soluble factors quantification.

1539    **Supplementary Movie 1.** RSCM image acquisition along with 3-Dimensional rendering of

1540    gross whole eye morphology and cross-sectional image acquisition showing infiltrating red

1541    CMTPX-tagged neutrophils in the retina and Schlemm's canal (a channel at the limbus, which is

1542    the joining point of the cornea and sclera, encircling the cornea) among intravenously injected

1543    NOD-SCID mice treated with IFNλ-exposed WT neutrophils.

1544